Title
SEMICONDUCTOR VARIABLE DELAY ELEMENTS.

Author
Tuyl, Rory Lynn. Van

Publication Date
1968-12-01

UCRL-18668

cy. 2

SEMICONDUCTOR VARIABLE DELAY ELEMENTS

Rory Lynn Van Tuyl
(M.S. Thesis)

December 1968

LAWRENCE RADIATION LABORATORY
UNIVERSITY of CALIFORNIA BERKELEY

UCRL-18668

cy. 2

DISCLAIMER

UCRL-18668

UNIVERSITY OF CALIFORNIA

Lawrence Radiation Laboratory
Berkeley, California

AEC Contract No. W-7405-eng-48

SEMICONDUCTOR VARIABLE DELAY ELEMENTS

Rory Lynn Van Tuyl
(M. S. Thesis)

December 1968

ABSTRACT

This paper is concerned with electronic devices which exhibit the property of controllable signal propagation delay based on the principle of minority carrier drift in semiconductors.

Theoretical predictions of the time domain response of ideal devices are compared to measurements made on a practical device fabricated with the gaseous diffusion techniques used in the manufacture of integrated circuits.

The theoretical aspects of temperature compensation are discussed, and successful temperature compensation of a device is reported.

Application of devices to time delay, phase-shift, frequency selective filter, and oscillator circuits are presented, and the course of future work, leading to more sophisticated applications is outlined.

CONTENTS

LIST OF SYMBOLS

A = Area

$a = t_0/2K^2$

d = Emitter-to-collector spacing

D_p = Hole diffusion constant

D_n = Electron diffusion constant

$\mathcal{E}$ = Electric field

I = Current

I_s = Sweeping current

I_o = Output current

I_i = Input current

J = Current density

$J_{(Drift)}$ = Drift current density

$J_{(Diff)}$ = Diffusion current density

J_n = Electron current density

J_p = Hole current density

$j = \sqrt{-1}$

K = Standard deviation of Gaussian (in units of time)

$\frac{kT}{q}$ = Thermal voltage

L = Length

$\mathcal{L}$ = Laplace Transform

$\mathcal{L}$ = Diffusion length

ℓ = Length

n = Volume electron density

n' = Excess volume electron density

N_o' = Excess initial area electron density

N_A = Acceptors per unit volume

N_D = Donors per unit volume

p = Volume density of holes

p' = Excess volume density of holes

P = Power

Q = Q Factor of resonant circuit

Q = Charge

Q_o = Injected charge

q = Electronic charge

R = Resistance

R_D = Device resistance

R_S = Temperature sensing resistance

s = Laplace operator

t = Time

t_D = Pulse delay time

T_o = Input pulse time duration

T = Temperature

V = Voltage, voltage applied to device

V_S = Temperature sensing voltage

v = Velocity

W = Width

W_t = Width (in time)

W_e = Emitter width

ΔW_t = Change in time width

X = Distance variable

α = Common base current transfer ratio

β = Common emitter current transfer ratio

$\delta(t)$= Unit impulse function

ϵ = Dielectric permittivity

μ = Mobility

μ_p= Hole mobility

μ_n= Electron mobility

μ^*= Effective mobility

ρ = Resistivity

σ = Conductivity

τ_R= Dielectric relaxation time

τ_n= Minority lifetime of electrons

ω = Radian frequency

INTRODUCTION

The direct observation of minority carrier drift, diffusion, and recombination in semiconductors was first reported in 1950 by Haynes and Shockley. Their work, undertaken in connection with the early transistor development program, laid the experimental foundation for the theory by which we now understand semiconductor devices. One of the most striking features of this experiment was the controllable delay of electrical signals made possible through the mechanism of minority carrier drift. The highly successful application of minority carrier transport in amplifying and switching devices has overshadowed the time delay property which has found little or no application in the years since the original experiment.[1]

This paper discusses the theoretical aspects of a device based on these principles, the successful fabrication and testing of such a device, the relation of test results to theoretical predictions, and the possibilities for practical application of devices which fall into this class of Semiconductor Delay Elements.

PRINCIPLES OF CARRIER TRANSPORT[2]

Majority carriers in semiconductors such as silicon and germanium behave similarly to free carriers in materials commonly called conductors. The movement of carriers under the influence of an electric field is given by:

(1)

$$J = \sigma \mathcal{E} .$$

J = current density
$\mathcal{E}$ = electric field
σ = conductivity

The one-dimensional steady-state motion of holes under an electric field in a p-type semiconductor, for instance, is described by:

(2)

$$J_{P(DRIFT)} = q P \mu_P \mathcal{E},$$

$J_{P(DRIFT)}$ = drift current
P = hole density
q = electronic charge
μ_P = hole mobility

where ($q P \mu_P$) can be recognized as the conductivity by comparison of (1) and (2). The velocity of hole motion (from the principle that $J = d(Q/A)/dt$) is:

(3)

$$v = \mu_P \mathcal{E} .$$

A = unit area
v = hole velocity

Majority carriers also move, or diffuse, under the influence of concentration gradients.

(4)

$$J_{P(DIFF)} = -q A \frac{\partial P}{\partial X}$$

D_P = diffusion constant for holes
$J_{P(DIFF)}$ = hole diffusion current
X = dimension under consideration

When this aspect of semiconductor conduction is considered, the total expression for current becomes:

(5)

$$J_p = J_{p(DIFF)} + J_{p(DRIFT)} = -qD_p\frac{\partial p}{\partial x} + qp\mu_p\mathcal{E} .$$

As far as transient phenomena are concerned, majority carriers are similar to free carriers in conductors. In both cases, the length of time for which an un-neutralized space charge region can exist after the injection or withdrawal of a quantity of free carriers is very short. The charge-unbalanced region decays exponentially with characteristic time

(6)

$$\tau_R = \frac{\epsilon}{\sigma},$$

σ = conductivity

ϵ = permittivity

called the dielectric relaxation time. For silicon and germanium, the relaxation time is of the order of a picosecond for $1\ \Omega\text{-cm}$ material.[3] This is the time interval during which large majority currents flow from an external source in contact with the material to extinguish the charge-produced electric field. For purposes of signal delay, therefore, majority carriers provide negligible increase in delay over that which is obtainable with electromagnetic waves. So any hope for a practical delay device depends on minority carrier behavior.

Minority carriers, for instance electrons in a p-type semiconductor, obey the same conduction laws with respect

to drift and diffusion as do majority carriers. So,

(7)
$$J_n = q D_n \frac{\partial n}{\partial x} + q \mu_n n \mathcal{E}$$

in the one-dimensional case being considered.

Minority carriers are not free, however, to flow in and out of contacts by displacement as do majority carriers. But the rules of space charge quasi-neutrality still apply. What happens is that an excess of minority carriers over the thermal equilibrium value is space-charge neutralized by majority carriers in the interval of the relaxation time, and then the two species of carrier recombine in approximately exponential fashion with characteristic time τ_n, called the lifetime of minority carriers in the material.

Therefore,

(8)
$$n' = n'(t=0)\, e^{-t/\tau_n},$$

n' = excess minority concentration above thermal equilibrium.

$n'(t=0)$ = initial excess minority carrier concentration

and, differentiating:

(9)
$$\frac{dn'}{dt} = -\frac{n'}{\tau_n}$$

Since the concentration of majority carriers must closely follow that of the minority carriers in order to preserve space charge quasi-neutrality:

(10)

$$\frac{d\rho'}{dt} = -\frac{\rho'}{\tau_n} .$$

The three previously considered phenomena (drift, diffusion, and recombination) can now be combined into two equations expressing the conservation of charge, known collectively as the continuity equation, which describe the time behavior of minority and majority carriers in a semiconductor. Because $\partial\rho = \partial\rho'$ and $\partial n = \partial n'$, the resulting expressions are:

(11)

$$\frac{d\rho_p'}{dt} = \frac{1}{q}\frac{\partial J_p}{\partial x} - \frac{\rho'}{\tau_n} = -D_p\frac{\partial^2\rho'}{\partial x^2} + \mu_p\mathcal{E}\frac{\partial\rho'}{\partial x} - \frac{\rho'}{\tau_n}$$

(12)

$$\frac{dn_p'}{dt} = \frac{1}{q}\frac{\partial J_n}{\partial x} - \frac{n'}{\tau_n} = D_n\frac{\partial^2 n'}{\partial x^2} + \mu_n\mathcal{E}\frac{\partial n'}{\partial x} - \frac{n'}{\tau_n}$$

Now consider the case where an impulse of minority carriers is injected into a semiconductor. First, charge neutrality is provided virtually instantaneously, so that an excess of holes and electrons exists in the region of injection. Second, these carriers tend to spread out due to the concentration gradients. Third, the holes and electrons tend to recombine, thereby reducing the density of the concentration lump with the time constant . Fourth, if an externally applied drift field is present, the concentration lump moves in the direction in which charges of like sign with the minority carriers would

move in such a field. This illustrates the dominance of minority carriers over majority carriers in the process of excess carrier drift.

The velocity with which the lump moves is

(13) $$v = \mu_n \mathcal{E} .$$

This equation is well obeyed in silicon up to velocities of about 2×10^6 cm/sec.[4]

It can be seen, then, that reasonable delays can be obtained in micron distances with velocities ranging from 10^4 to 10^6 cm/sec. Of course the maximum delay obtainable is governed by the lifetime, both at the material surface and in the bulk, which is of microsecond duration even in the most perfect samples. Lifetimes can be reduced to the order of a nanosecond in samples with poor surface properties or a high density of bulk recombination centers, as with gold doping.

The solution of the continuity equation for minority carriers can be obtained under the following assumptions:[5]

1) One-dimensional solution
2) Unit impulse excitation in both time and space
3) Substantial conductivity (i.e. short τ_R)
4) Extrinsically doped sample
5) Low level injection (minority injection much smaller than majority doping)

The solution under these conditions is:

(14)

$$n'(x,t) = \frac{N_o'}{2\sqrt{\pi D_n t}} \; e^{-\frac{t}{\tau_n}} \; e^{-(x-\mu_n \mathcal{E} t)^2/4D_n t} .$$

N_o' = Initial area concentration of minority carriers

$n'(x,t)$ = Volume density of minority carriers as a function of distance and time

This equation can be recognized as a gaussian distribution in the moving coordinate system x', where

(15)

$$x' = (x - \mu_n \mathcal{E} t) .$$

The Haynes-Shockley experiment was originally performed with holes in n-type germanium crystal, using a point contact emitter and collector. Delays of tens of microseconds duration were obtained in germanium crystals with measured lifetimes as high as 200 μsec and mobility measured to be $\cong$ 1.7 x 10^3 cm^2/volt-sec.[6] This classic experiment illustrated conclusively the existence of hole and electron drift, diffusion, and bulk and surface recombination, as well as providing an accurate and direct measurement of drift mobility of minority carriers.

IDEAL DEVICE CHARACTERISTICS

Before considering the practical aspects of exploiting the Haynes-Shockley experimental results, let us examine more closely the predicted behavior of an ideal device.

Figure 1 shows a diagram of (a) an ideal device and the carrier distributions existing in space a finite time after the injection of (b) an impulse of minority carriers and (c) a step of minority carriers. If we neglect the effect of the difference in time between the collection of the first carriers in the packet and the last, we can transform (14) into a function of t and t_D:

(16) $$F(t) = \left|\frac{I_o}{I_i}\right| = \frac{T_o}{2\sqrt{\pi}K + T_o}\, e^{-t_o/\tau_n}\, e^{-(t-t_D)^2/4K^2}$$

I_o = output current

I_i = input current

$K = \frac{\sqrt{D_n t_D}}{v}$ = standard deviation of a gaussian pulse (in units of time)

T_o = input pulse duration

In the case of a unit current impulse, where $I_i = Q_o\,\delta(t)$:

(17) $$I_i\, T_o = Q_o\, \delta(t)\, T_o = Q_o . \quad (T_o \to 0)$$

$\delta(t)$ = unit impulse function

Q_o = injected charge

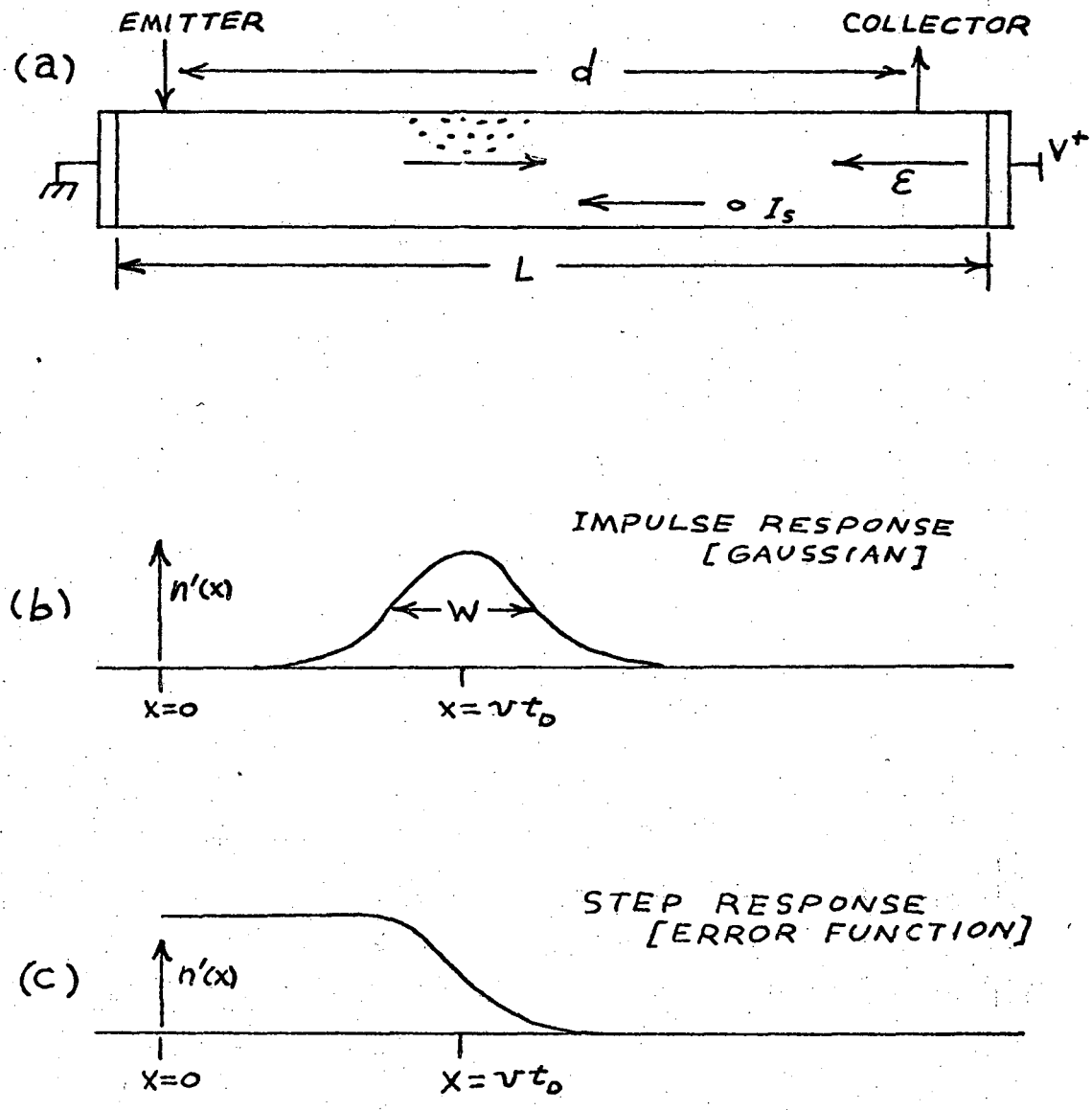

FIGURE 1

(a) Diagram of an idealized device

(b) Carrier distribution in space at time t_D due to unit impulse input

(c) Carrier distribution in space at time t_D due to unit step input

Therefore:

(18) $$I_o = \frac{Q_o}{2\sqrt{\pi}K} e^{-\frac{t_o}{\tau_n}} e^{-(t-t_o)^2/4K^2}$$

which is the pure gaussian form.

The pertinent features of the resulting pulse are the width, amplitude, and delay. A description of these properties is contained in (16). First, we will consider delay.

(19) $$t_D = \frac{d}{v}$$

where: t_o = delay to center of gaussian or to half maximum amplitude of erf response

d = distance from emitter to collector

So, for fixed d, and variable applied drift field:

(20) $$t_D = \frac{d}{v} = \frac{d}{\mu_n \mathcal{E}} = \frac{d}{\mu_n (\frac{V}{L})} = \left(\frac{Ld}{\mu_n}\right) V^{-1}$$

V = applied drift voltage

L = distance between ohmic contacts

For fixed applied voltage, and variable d:

(21) $$t_D = \left(\frac{L}{\mu_n V}\right) d^{+1}$$

Next, consider the width of the concentration lump, expressed in units of time:

(22)
$$W_t = \frac{We}{v} + T_o + \Delta W_t$$

Where:

W_e = emitter width

T_o = input pulse duration

ΔW_t = width increase due to diffusion of minority carriers away from the region of high excess concentration.

(23)
$$\Delta W_t = \frac{\sqrt{11.1\, D_n t_o}}{v} = \sqrt{11.1}\, K$$

where ΔW_t is taken as the width increase measured at one-half the maximum amplitude (FWHM), and $\sqrt{11.1}$ is the conversion factor from standard deviation to FWHM.[7]

So, for a fixed emitter-to-collector spacing, and variable drift field:

(24)
$$\Delta W_t = \frac{\sqrt{11.1\, D_n}}{d} (t_D)^{3/2}$$

However, for a fixed drift field and variable distance:

(25)
$$\Delta W_t = \frac{\sqrt{11.1\, D_n}}{v} (t_D)^{1/2}$$

Equations (24) and (25) are alternate forms of the basic relation expressed in (23), but with different parameters held constant and delay time as the independent variable. These forms are those most easily compared with experimental results.

Attenuation is the result of two effects, diffusion and recombination. In the absence of recombination, we would expect the product of pulse amplitude and width to remain constant, since the total number of injected carriers is constant in time. Therefore, considering diffusion only:

(26) $$\left|\frac{I_o}{I_i}\right| \propto \frac{1}{2\sqrt{\pi D_n t_o} + \nu T_o}$$

If we multiply by the recombination term to take care of carrier loss:

(27) $$\left|\frac{I_o}{I_i}\right| \propto \frac{e^{-t_o/\tau_n}}{2\sqrt{\pi D_n t_o} + \nu T_o}$$

Furthermore, the amplitude is proportional to input pulse duration, leading us to:

(28) $$\left|\frac{I_o}{I_i}\right| = \frac{\nu T_o}{2\sqrt{\pi D_n t_o} + \nu T_o} e^{-t_o/\tau_n}$$

or, for unit impulse excitation,

(29) $$I_o = \frac{\nu Q_o}{2\sqrt{\pi D_n t_o}} e^{-t_o/\tau_n}$$

Notice that as $T_o \rightarrow \infty$ in equation (28), the transfer

function approaches its dc value:

(30)

$$\left|\frac{I_o}{I_i}\right|_{dc} = e^{-t_D/\tau_n}$$

Figure 2 is a set of graphs summarizing the time response relationships described here. These graphs form a basis for comparison with the experimental data, which is given later in the paper.

Since the response function of an ideal semiconductor delay device would obviously be a low pass characteristic with variable phase shift, an examination of the frequency response should yield some interesting information.

We can determine the frequency response by taking the Laplace transform ($\mathcal{L}$) of the time response to a unit impulse:

(31) $\mathcal{L}$ (Impulse response) = F(s).

F(s) = transfer function in s, the Laplace variable.

From (18):

(18)

$$I_o = F(t)\, Q_o\, \delta(t) = Q_o\left[\frac{1}{2\sqrt{\pi}K}\, e^{-t_D/\tau_n}\, e^{-(t-t_D)^2/4K^2}\right]$$

which becomes, on expanding the exponent:

(18a)

$$F(t)\, Q_o\, \delta(t) = Q_o\, \frac{e^{-t_D/\tau_n}}{2\sqrt{\pi}K}\left[e^{-t^2/4K^2}\, e^{2t\,t_D/4K^2}\, e^{-t_D^2/4K^2}\right]$$

FIGURE 2 CAPTIONS

(a) Pulse delay time, t_D, as a function of control voltage, for a fixed emitter-to-collector spacing.

(b) Pulse delay time, t_D, as a function of emitter-to-collector spacing, for a fixed control voltage.

(c) Pulse width increase, ΔW_t, as a function of time delay, with fixed emitter-to-collector spacing and variable control voltage.

(d) Pulse width increase, ΔW_t, as a function of time delay, with fixed control voltage and variable emitter-to-collector spacing.

(e) and (f) Current transfer function $\left|\frac{I_o}{I_i}\right|$, as a function of time delay. Upper curve attenuation due to diffusion only, lower curve shows combined effect of diffusion and recombination.

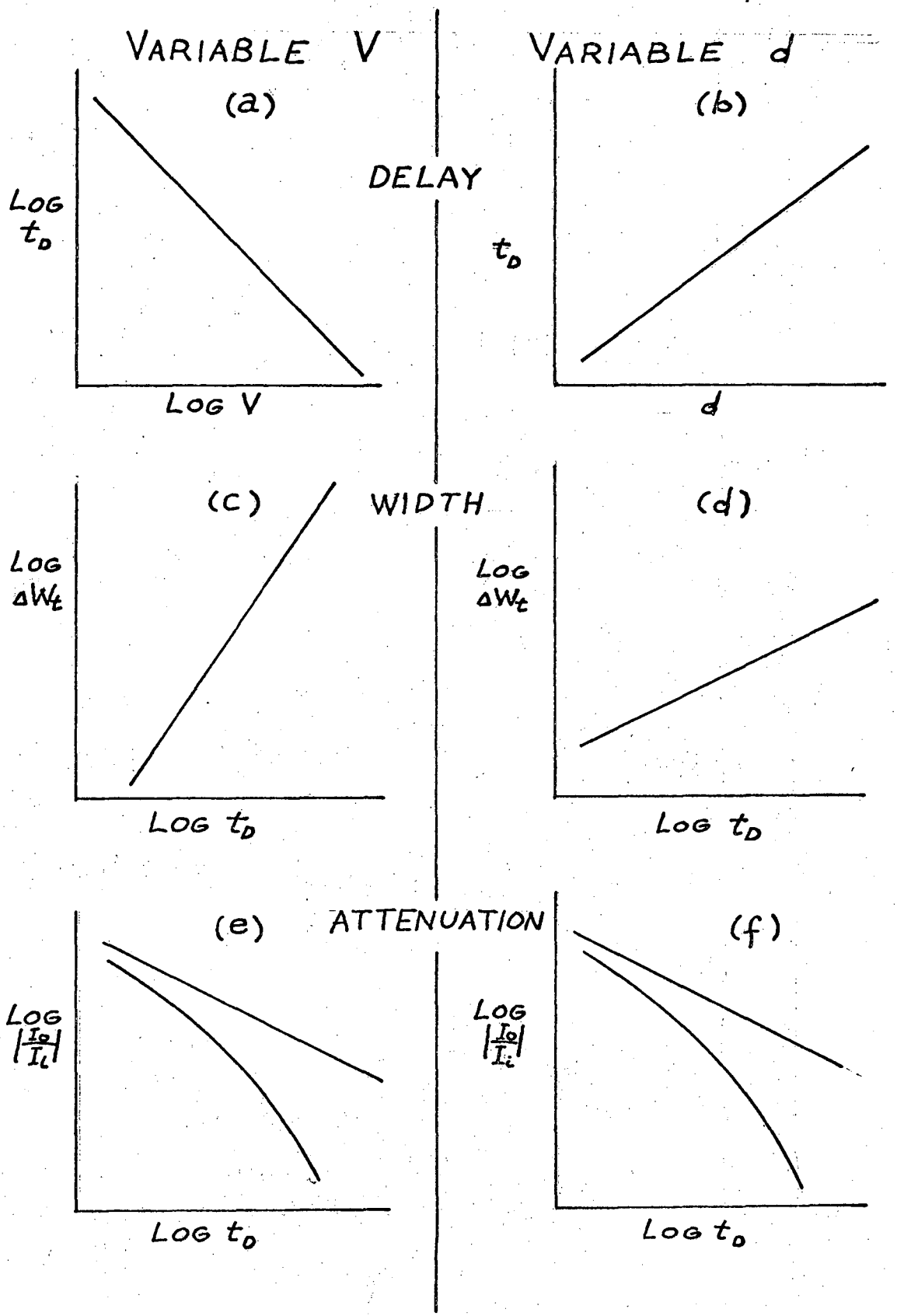

FIGURE 2 – TIME DOMAIN RESPONSE

Let

(32) $$a = t_D/2K^2$$

Then (18) can be expressed as:

(18b) $$F(t)\,Q_o\,\delta(t) = Q_o\left(\frac{e^{-t_D/\tau_n}e^{-t_D^2/4K^2}}{2\sqrt{\pi}K}\right)\left(e^{-t^2/4K^2}\right)\left(e^{at}\right)$$

But:

(33) $$\mathcal{L}\left[F(t)\,e^{at}\right] = F(s-a)$$ [8]

Therefore

(34) $$F(s-a) = \left[\frac{e^{-t_D/\tau_n}e^{-t_D^2/4K^2}}{2}\right]\left[e^{K^2(s-a)^2}\,\mathrm{erfc}\left(K(s-a)\right)\right]$$ [9]

Recall that, from (23), the conversion between standard deviation and pulse width is:

(23) $$W_t = \sqrt{11.1}\;K,$$

so that an alternative expression of (34) is:

(34a) $$F(s-a) = \left[\frac{e^{-t_D/\tau_n}e^{-2.8\left(\frac{t_D}{W_t}\right)^2}}{2}\right]\left[e^{\frac{W_t^2\left(s-\frac{5.5t_D}{W_t^2}\right)^2}{}}\,\mathrm{erfc}\left[\frac{W_t}{3.3}\left(s-\frac{5.5t_D}{W_t^2}\right)\right]\right]$$

The frequency response can be determined by setting $s=j\omega$ in equation (34) and obtaining the magnitude and phase of

$F(j\omega - a)$ as ω varies.

The function F(s-a), given by (34) is tabulated in several references,[10] but most usefully in Fried and Conte. The details concerning the application of this function are given in the appendix, so only the results are presented here. Figure 3a is a normalized plot of the frequency sensitive portion of F(s-a) in polar form, for various ratios of time delay to pulse width.[11] Devices with high ratios of t_D/W_t are best for pulse delay applications, since this implies maximum bandwidth for a given delay. Devices with low ratios of t_D/W_t are best for most phase-shift applications, since attenuation of harmonics above the frequency of interest is maximum.

Examination of the amplitude versus frequency plot in Figure 3b reveals an extremely sharp cut-off characteristic for a typical value of t_D/W_t. Such a characteristic could be very useful if adequate control and stability of device parameters could be achieved.

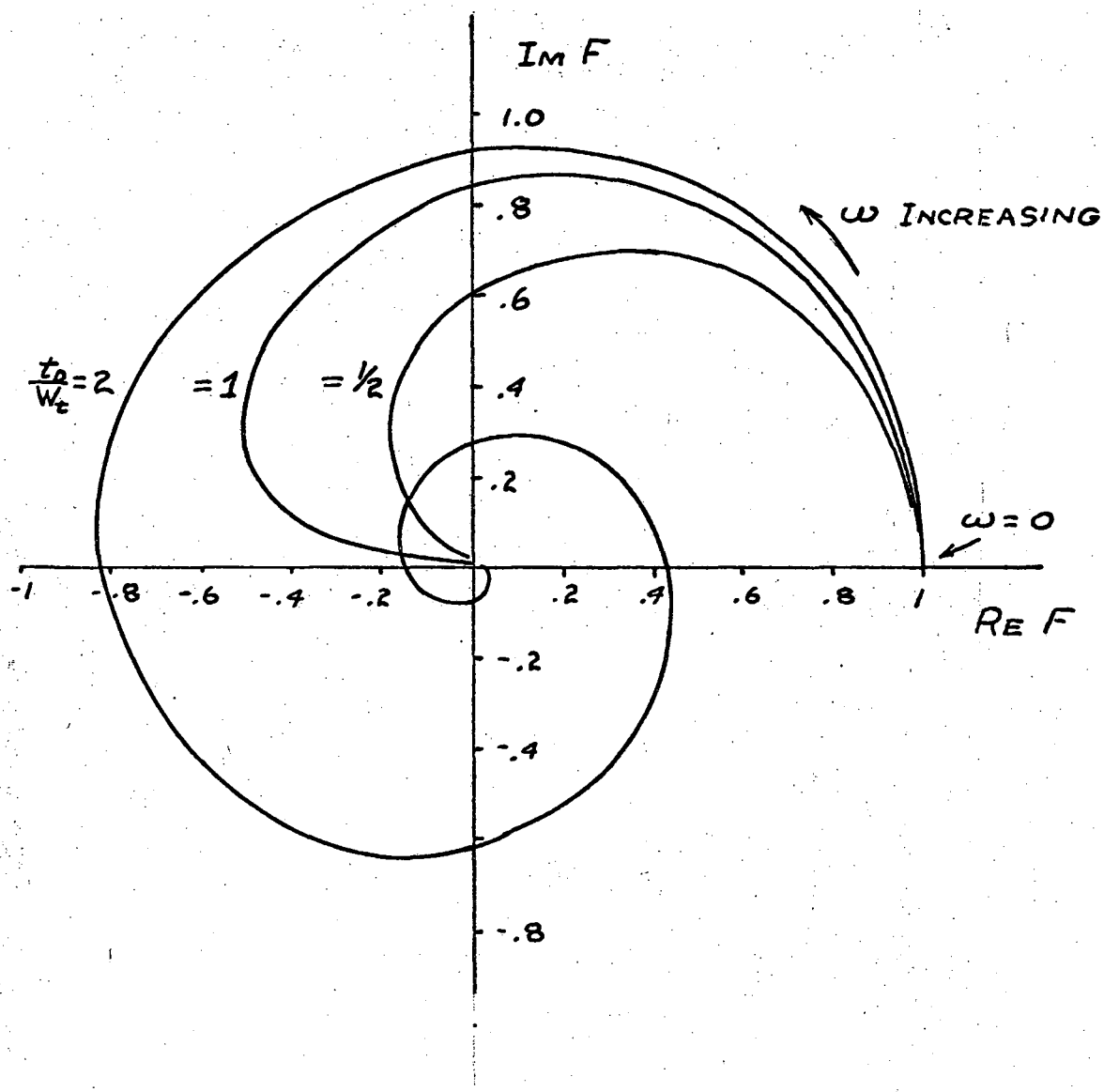

FIGURE 3a : $F(j\omega - a)$ [NORMALIZED]

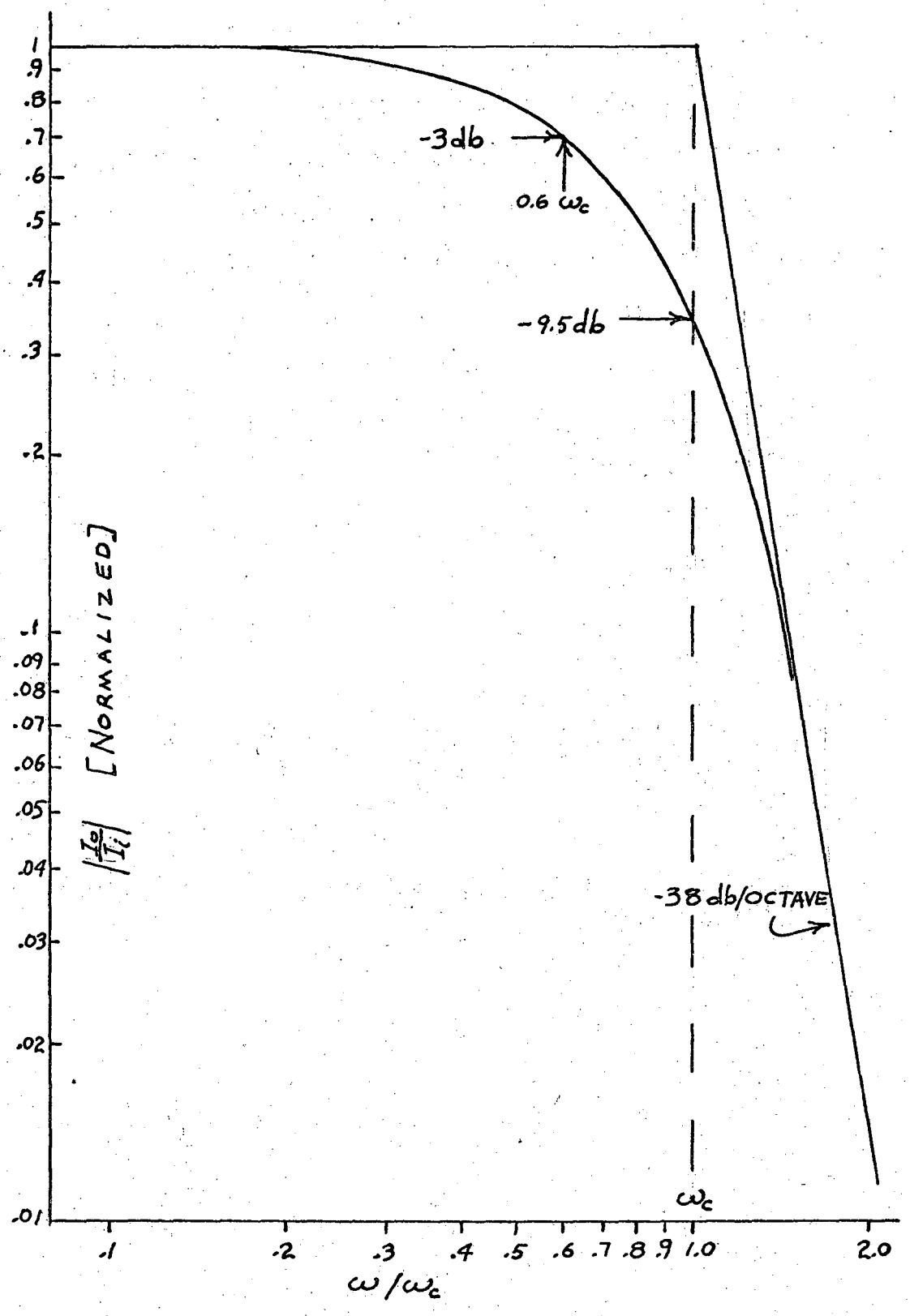

FIGURE 3b : $|F(j\omega - a)|$ FOR $t_0/w = 1.13$
[THEORETICAL]

DESIGN AND FABRICATION

The design of a device to meet the goals of this project represented a compromise between the ideal situation, the practical limitations of the diffused technology, and the capability of existing fabrication facility.[12] The goal was to produce a device with delays of tens to hundreds of nanoseconds, maximizing bandwidth, and minimizing attenuation.

For these relatively short delays, the velocity of carriers should be of the order of 10^5 to 10^6 cm/sec. Obtaining this high a velocity required the selection of the highest mobility silicon available so that electric fields could be kept within reasonable limits. The highest mobility for minority carriers is found in p-type silicon with doping levels less than 10^{15} atoms/cm^3. The mobility in this material decreases from greater than 1000 cm^2/volt-sec at 10^{15} atoms/cm^3 to about 300 cm^2/volt-sec at doping levels above 10^{17} atoms/cm^3.[13] A velocity of 10^6 cm/sec requires a field of 10^3 volts/cm with a mobility of 1000 cm^2/ volt-sec. Silicon wafers with doping levels of 10^{14} atoms/cm^3 and lifetimes in excess of 1 microsecond were chosen for the basic material.

The geometry of the device was planned to provide five n-type emitters and one n-type collector in a line between ohmic field-producing contacts in the p-type background.

Diffusing n on p junctions into lightly doped material is not practical because of the ability of surface state charges and surface oxides containing positive ions to invert the lightly doped material at the surface, producing a thin n-type layer which forms a conducting path between n-type diffusions.[14] To overcome this effect, a channel of boron-doped p material was diffused into the lightly doped background to form a "Guard-ring" around all n-type diffusions. "Base" contacts were made adjacent to each emitter so that a low-resistance path existed for effective forward-biasing of the emitter junctions. Figure 4 is a photograph of the device showing the five emitters, the five "bases" and the collector, situated between the ohmic field-producing contacts. Notice that the base contacts are placed beside the emitters to avoid areas of extremely high surface recombination velocity in the signal flow path.

One of the main design considerations involved keeping the surface recombination to a minimum. It was assumed that surface recombination centers would substantially reduce the lifetime of electrons below the 1 μsec bulk lifetime, so the channel diffusion was planned to force minority carriers away from the surface, utilizing the built-in drift field which results from doping concentration gradients. Using the assumption of an exponential doping profile

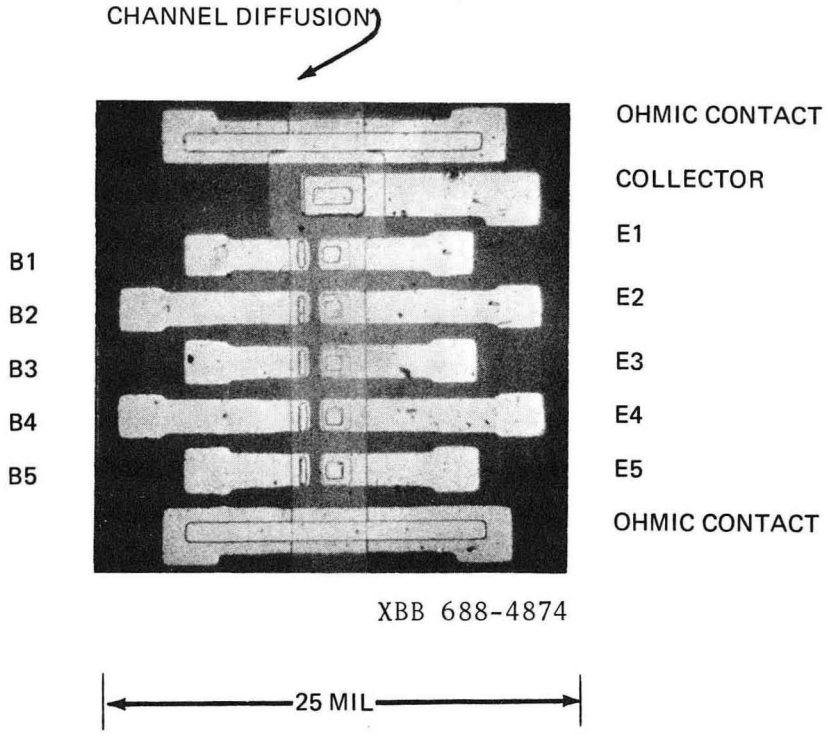

FIGURE 4: COMPLETED DELAY DEVICE

(35)

$$P(x) = P_o e^{-x/\mathcal{L}}$$

P_o = surface doping concentration

$\mathcal{L}$ = diffusion length

The built-in electric field, $\mathcal{E}_{drift}$, is given by:

(36)

$$\mathcal{E}_{drift} = \frac{kT}{q} \cdot \frac{1}{\mathcal{L}} .$$

If a design value of $\mathcal{E}_{Drift} = 10^2$v/cm is chosen, a diffusion length of about 3 microns results. Choosing a surface concentration of about 10^{17} atoms/cm^3, a diffusion depth (at which doping becomes comparable to the bulk concentration of 10^{14} atoms/cm^3) of about 7 microns is obtained. The surface area covered by this p-type diffusion was made just large enough to cover the expected spreading area of the injected electrons, so that it would not lead to excessive power dissipation. In order to increase the collection efficiency, the n-type collector diffusion was made as deep as possible, of the order of 25 microns, so that carriers which diffused deep into the bulk could be collected. The emitters were required to be as shallow as possible, so that injection would take place at a junction of highly doped n and p type material. Figure 5 shows the doping profiles of the emitter, channel, and collector.

The problem of power dissipation becomes a serious one

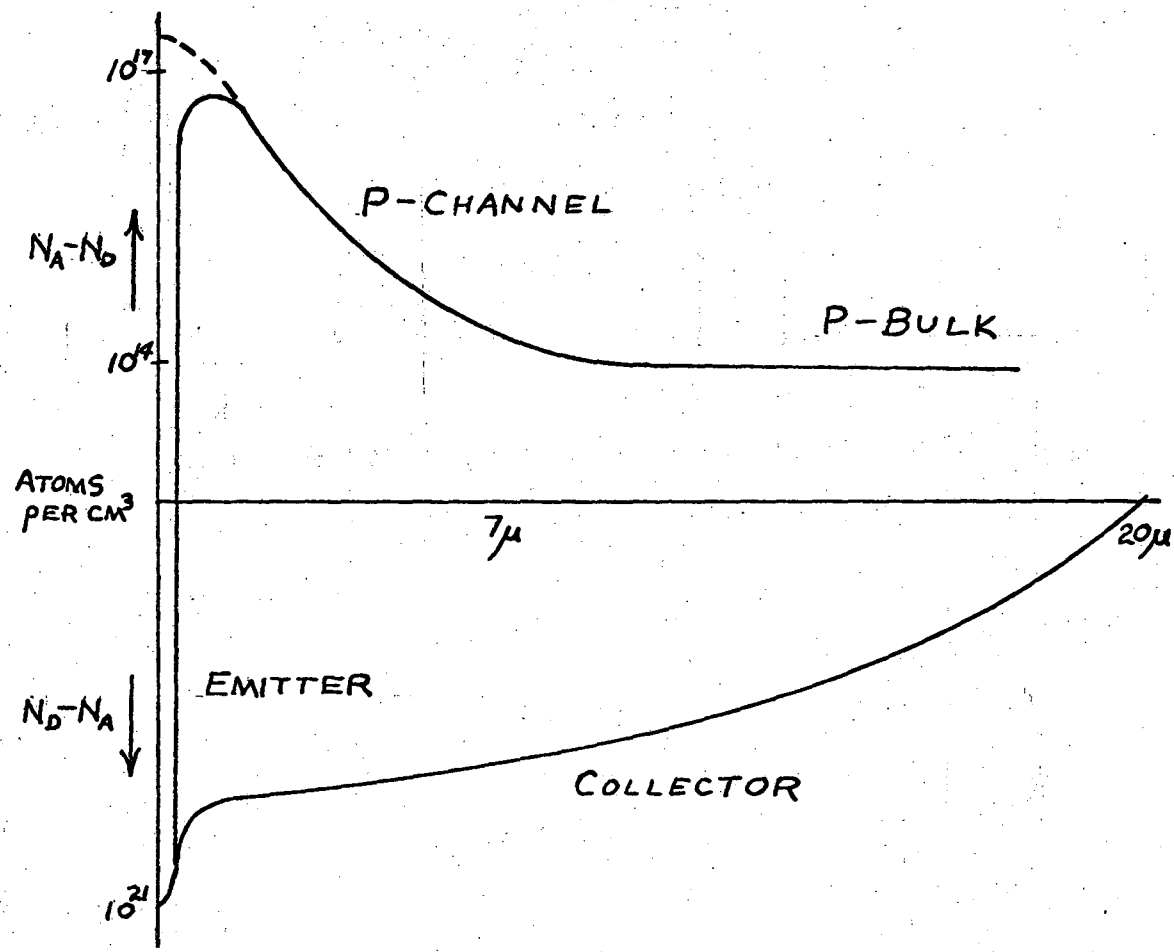

FIGURE 5 : ESTIMATED DOPING PROFILES

in devices of this type. Power dissipated in a bar of length ℓ, cross-section A, resistivity ρ, is:

(37)

$$P = \frac{V^2}{R} = \frac{\mathcal{E}^2 \ell^2}{\rho \ell / A} = \frac{\mathcal{E}^2 \ell A}{\rho}$$

$\mathcal{E}$ = desired electric field

It is therefore desirable to minimize the area and length of the chip, while maximizing the resistivity. The wafer thickness was minimized, and channel width limited, but the length between field-producing contacts was about 500 microns, requiring a voltage of 50 volts to give $\mathcal{E}$ = 1000 v/cm. A combined resistance of 5000 Ω for bulk and channel was aimed for, giving a maximum power dissipation of 0.5 watt at $\mathcal{E}$ = 1000 v/cm.

Some non-ideal aspects became apparent at the design stage, and the fabrication was undertaken with these in mind. First, the fact that the emitters were comparable in width to the distance between emitter and collector contacts meant that an electrical impulse input would be degraded into a carrier lump of finite width at the moment of injection.

The widening factor can be seen to be:

(38)

$$\frac{W_t(t=0)}{t_o} = \frac{We}{d}$$

We = emitter width

d = collector to emitter distance

The first emitter is the worst in this respect, and the last is the best. The first emitter, whose width is about equal to d would automatically give a pulse about equal in width to the delay time, even if diffusion were ignored. The effect is to seriously limit the maximum bandwidth of the device.

Second, the temperature dependence of mobility was recognized as a serious problem. The mobility decreases with increasing temperature, so that the device is subject not only to ambient temperature variations, but also to serious effects from heat produced by power dissipation in the chip. This effect de-sensitizes the delay to electric field. One common way to circumvent this problem is to pulse the drift field at low enough duty cycle so that self-heating becomes negligible. This, of course, has serious drawbacks in the operation of a useful device. Another possibility for correcting temperature dependence was planned at the design stage. If the temperature dependences of drift mobility (minority carriers) and conductivity mobility (majority carriers) are assumed to be equal, then biasing the device with a current source could be expected to produce temperature compensation.

The argument is as follows:

Since

(39)
$$v_e = \mu_n(T) \cdot \mathcal{E} ,$$

and

$$\mathcal{E} = \frac{I_s R}{\ell} = \frac{I_s\left(\frac{1}{q\mu_p(T)p}\right)\frac{\ell}{A}}{\ell} = \frac{I_s}{q\mu_p(T)pA} \tag{40}$$

v_e = velocity of electrons

I_s = "sweeping current"

R = device resistance

ℓ = length

A = area

then, if p is a constant, that is, no conductivity modulation takes place:

$$v_e = \frac{\mu_n(T)}{\mu_p(T)} \frac{I_s}{qpA} \tag{41}$$

So the more closely matched the temperature dependences of μ_n and μ_p, the more linear the relation between v_e and I_s.

The device described in this paper was fabricated with standard gaseous diffusion and photolithography techniques in the semiconductor laboratory of the Electronics Research Laboratory at the University of California, Berkeley. The starting wafer was a 100 Ω-cm (111) orientation p-type silicon wafer 20 mils thick. The wafer was lapped to less than 10 mils thickness, and the surface polished. The initial diffusion was for the n-type collector, producing an estimated junction depth of 20 microns with a 15-hour drive-in. Next was the channel diffusion, resulting in an estimated depth of 7 microns, a resistivity of 2×10^{-1} Ω-cm

(giving a surface concentration of about 4×10^{17} atoms/cm^3). This resulted in a combined resistance of 1.2 KΩ for the 10 KΩ bulk and 1.4 KΩ channel. This resistance was lower than hoped for, due to too large a channel doping level. The next step was the deposition of n^+ layers for emitters and also to cover the deep-collector deposit.

The devices were diced and mounted in 12-pin TO-5 headers for testing. The back of the chip, which was type n after processing, had to be electrically isolated from the header because it formed such a leaky junction that the ohmic properties of the device were disrupted by the large leakage currents. Bonding to the header was accomplished with non-conductive cement.

ELECTRICAL CHARACTERISTICS

The first electrical tests performed on the device were with a transistor curve-tracer. Two-terminal tests made between each emitter and nearest base contact showed "hard" (negligible reverse leakage current) junctions with reverse breakdown at about 9 volts. The collector-channel junction was also "hard" with reverse breakdown at about 15 volts. A two-terminal test on the field-producing contacts showed a linear V-I characteristic in both directions up to about 17v in either direction. At this point, the resistance abruptly changed from 1200 Ω to 200 Ω. This effect was probably due to some form of breakdown in the doped layers on the back of the chip, forming a lower resistance path between the ohmic contacts. The practical effect was to limit the continuous-mode operation of the device to voltages not much greater than 17 volts, because the low resistance greatly increased power dissipation at high voltages.

The similarity of this device to a lateral transistor is very close. A curve-tracer test using the emitter and base nearest the collector gave a typical set of common emitter curves. With no drift field applied, the common emitter current "Gain" was $\beta = 0.4$. The maximum obtainable was 1.4 with an applied drift field. This corresponds to a common-base current transfer ratio of $\alpha_{min} = 0.3$ and $\alpha_{max} = 0.6$. The improvement in α as the field is increased is due to the directing action of the drift field on the

minority carriers, as well as the reduced transit time due to drift, which reduces the effect of recombination. The curve tracer operated at 240 steps per second so these are essentially dc parameters. By analogy to a multi-emitter and base lateral transistor, the symbol shown in Figure 6 will be used throughout the paper in describing the performance of this device.

The basic arrangement for testing the impulse response, step response, and frequency response is shown in Figure 7. The drift field was switched on at a low enough duty cycle to minimize self-heating effects. The capacitors in the bases maintained a constant base voltage for high frequency and pulsed common-base operation. It was determined that increasing the collector reverse bias had little or no effect above a volt or so, therefore the self-reverse biasing effect of the circuit shown was sufficient to insure operation independent of collector-to-channel voltage.

Figure 8-a is a picture of the impulse response at a given drift field, resulting from inputs on emitters E1, E2, and E3. Notice that pulse from E3 looks a good deal more like the ideal gaussian response than those from E1 and E2. The reason for this is that E3 is far enough removed from the collector to more closely approximate the ideal assumptions. Figure 8-b shows the pulse from E2 for three different drift fields, but with amplitudes normalized to show more clearly the difference in delay. Figure 8-c shows the step response, which is approximately the same

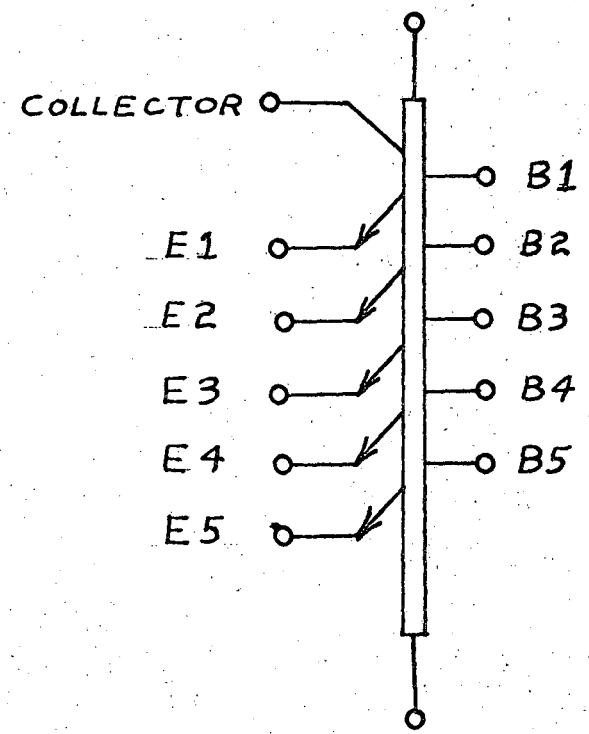

FIGURE 6: DEVICE SYMBOL

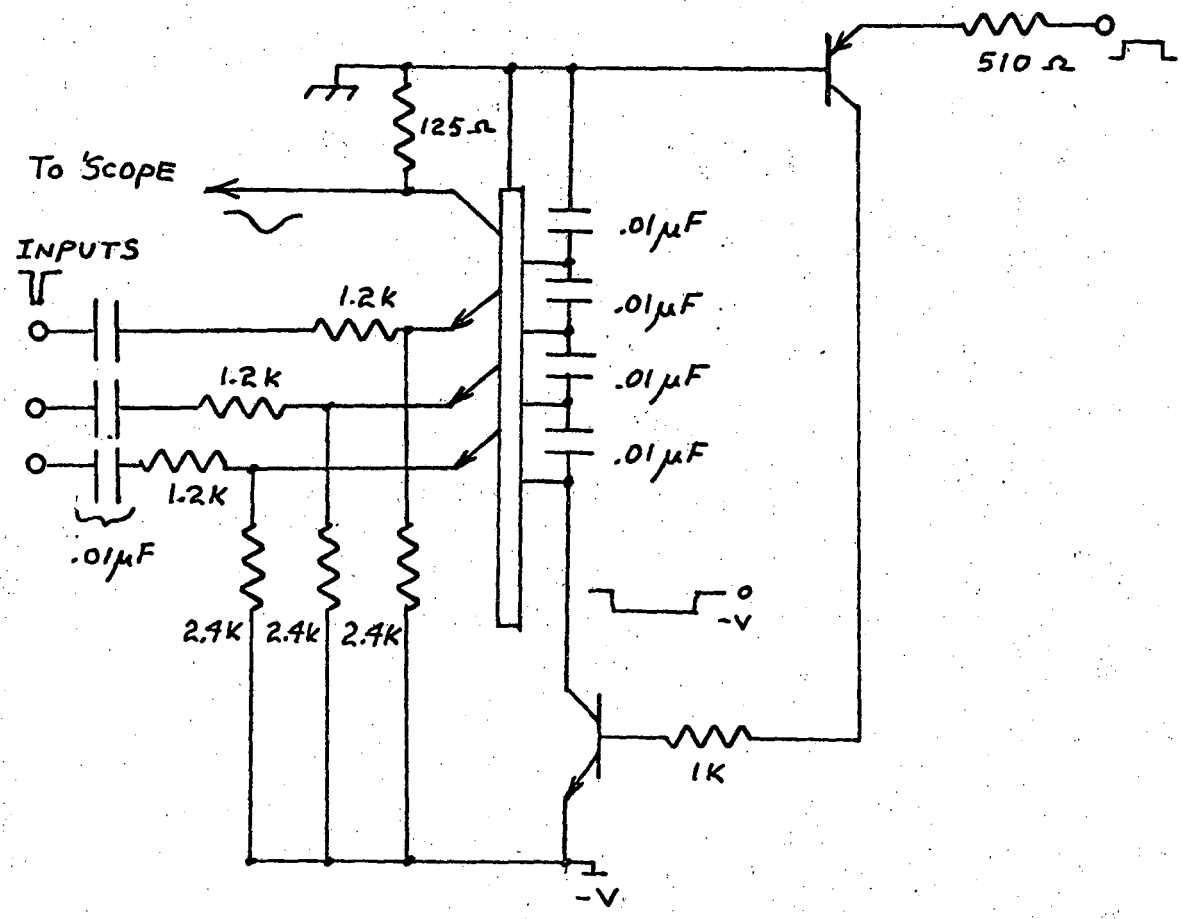

FIGURE 7: TEST CIRCUIT WITH PULSED DRIFT FIELD

(a)

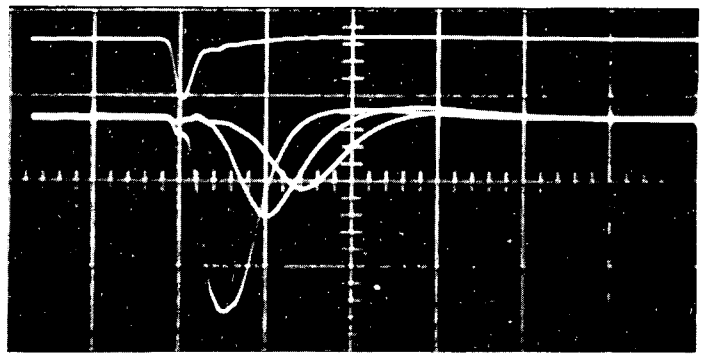

INPUT

OUTPUTS

FROM E1, E2, E3
AT V = 20 v.

50 NSEC/DIV.

(b)

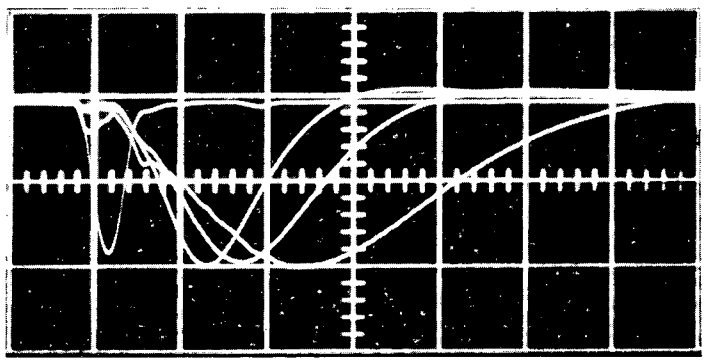

INPUT

OUTPUTS

FROM E2
AT V = 15v, 10v,
5v [AMPLITUDES
NORMALIZED]

50 NSEC/DIV.

(c)

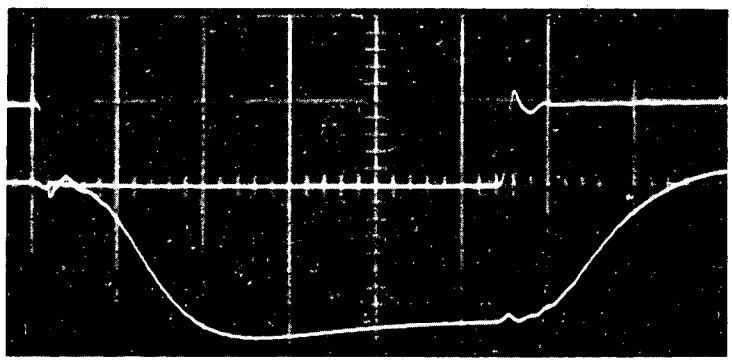

INPUT

OUTPUT

FROM E2
AT V = 13.5 v

50 NSEC/DIV.

XBB 688-4877-A

FIGURE 8: PULSE AND STEP RESPONSES

as the waveform obtained by Haynes and Shockley,[15] the integral of the gaussian, or error function.

Data was extracted from a series of photographs to see how well the time domain response agreed with the predicted response. Figure 9 shows delay as a function of distance for various applied drift voltages. This agrees well with the expected linear response predicted in Figure 2-b, when distance is measured from the center of each emitter to the near edge of the collector. Figure 10 shows delay as a function of applied drift voltage. There is a perplexing disagreement here between theory and experiment. Theory predicts (see equations 20 and Figure 2a) that delay should be proportional to $(V)^{-1}$, but experimental results show that it is proportional to $(V)^{-1/2}$. The practical effect of this relation is to make temperature compensation (discussed later) more difficult, and introduce an undesirable non-linearity into the control voltage.

It is interesting to extract a value for mobility from these data. The velocity can be obtained from the slope of the t_D-vs.-d curves in Figure 9. Using the calculated value of $\mathcal{E}$ and the relationship:

(42) $$\mu^* = v/\mathcal{E}$$

we get a value of μ^*, the effective mobility, which is plotted as a function of V in Figure 11. A satisfactory explanation for this apparent change in mobility would account for the anomalous relation between voltage and delay.

Figure 12 shows W_t, the pulse width at half amplitude,

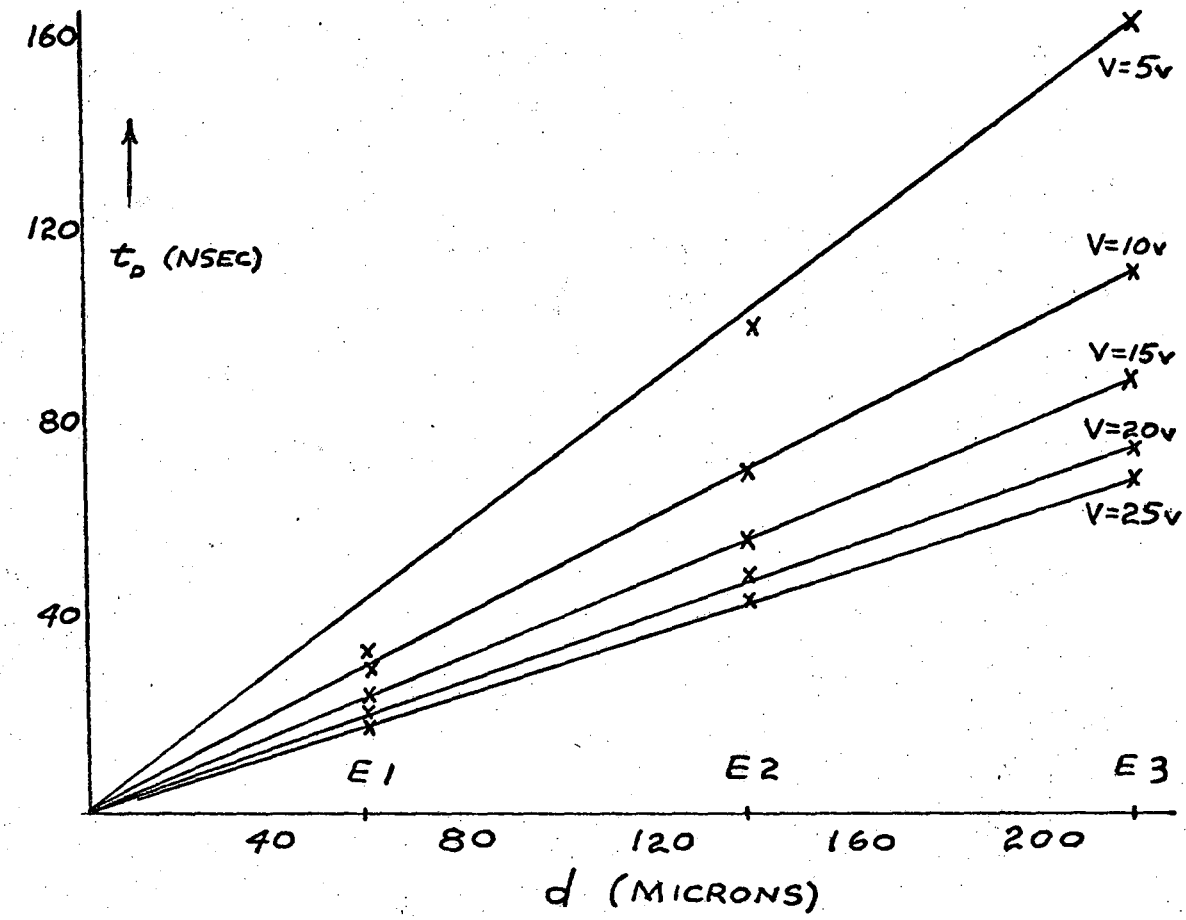

FIGURE 9: DELAY-VS-DISTANCE

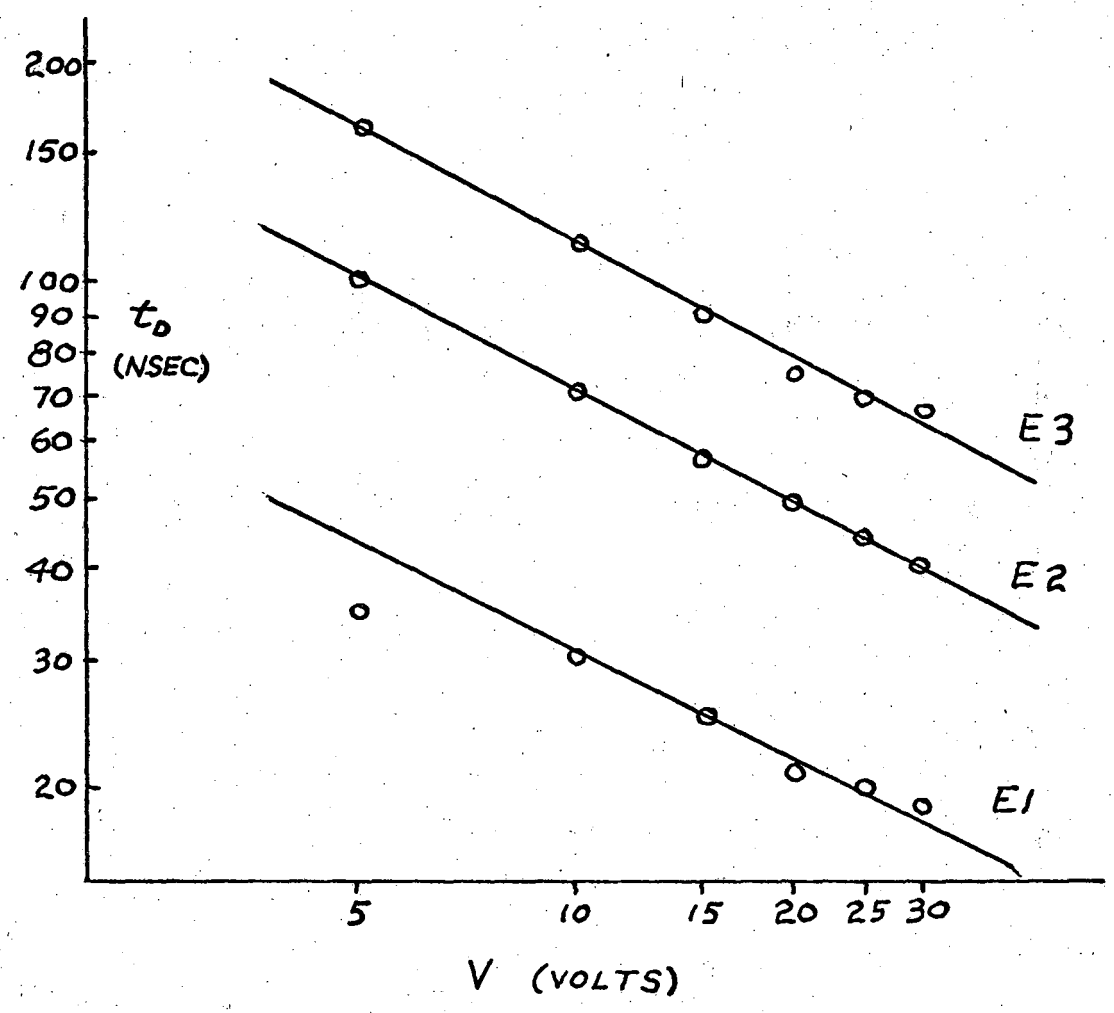

FIGURE 10: DELAY -VS- APPLIED VOLTAGE

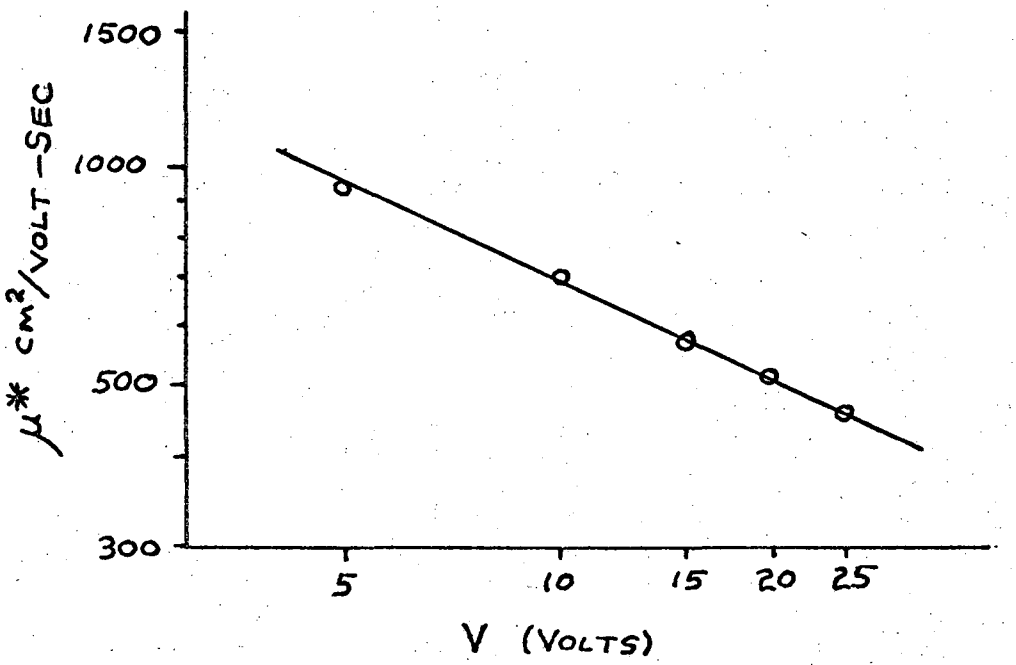

FIGURE 11: APPARENT MOBILITY-VS-VOLTAGE

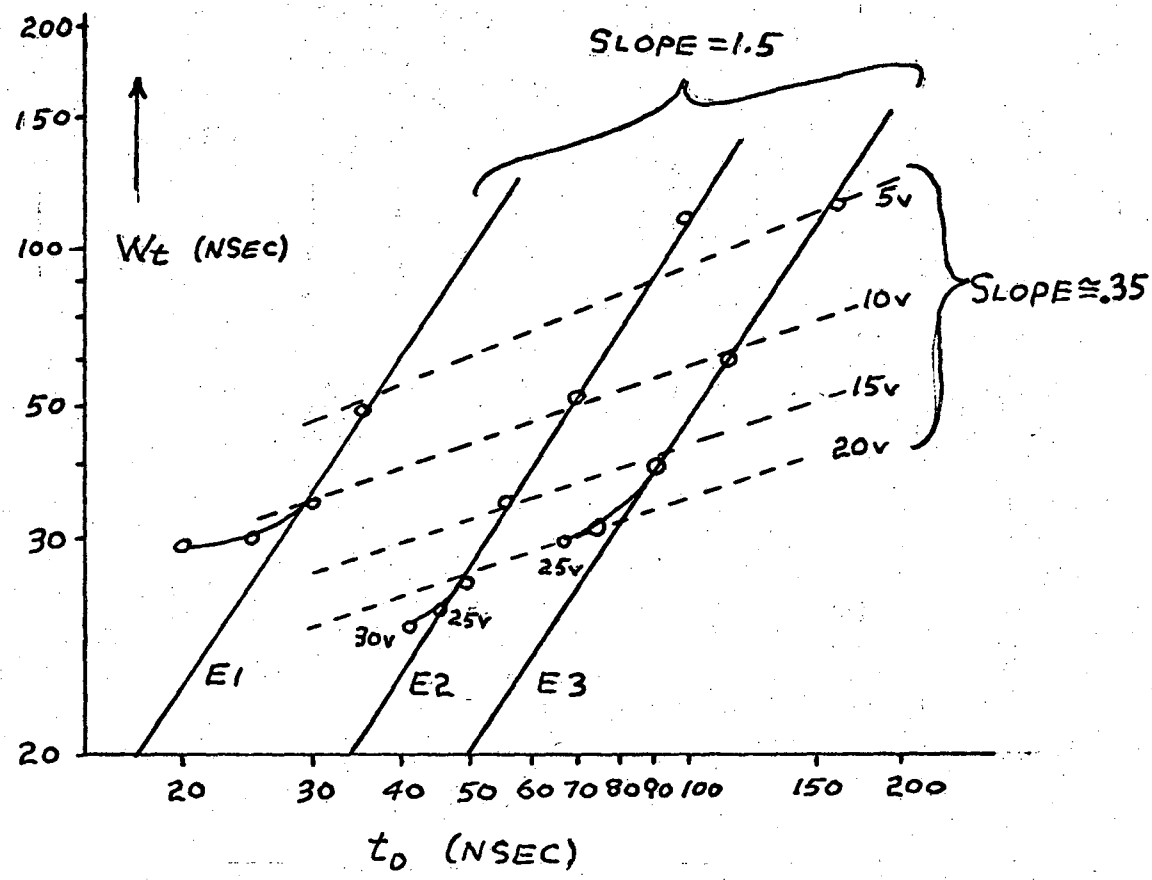

FIGURE 12: OUTPUT PULSE WIDTH -VS- DELAY

plotted as a function of t_D. The lines of constant distance for E1, E2, E3, show excellent agreement with the 3/2-power relation illustrated in Figure 2-c. There is a departure from this law as the delay becomes smaller. This is to be expected because the pulse width becomes more a function of emitter width and less a function of diffusion as the time of travel becomes smaller. The dotted lines through the points of equal drift voltage agree less well with the predicted relation shown in Figure 2-d. The actual slope is 0.35, as opposed to the theoretical 0.5, but this error could be due to the initial width, which is comparable to the output pulse width at shorter delay times.

The fact remains that the pulse widening is far greater than anticipated for the delay obtained. On purely theoretical grounds the width should be that expressed in (22),

(22) $$W_t = \frac{We}{v} + T_o + \frac{\sqrt{11.1\, D_n t_o}}{v}$$

Taking typical values for the parameters in the above expression, as inferred from other measurements:

For $t_D = 70$ nsec

$W = 62$ nsec

at E2, V = 10v

$T_0 = 10$ nsec

$W_e = 50 \times 10^{-4}$ cm

$v = 2 \times 10^5$ cm/sec

We get:

$$D_n = 67 \text{ cm}^2/\text{sec (measured)}.$$

But we know that the temperature is near 25°C, and the effective mobility is 700 cm^2/volt sec, therefore:

$$D_n = 18 \text{ cm}^2/\text{sec (calculated)}.$$

The measured spreading, which is almost four times the predicted value, forms the single most limiting defect in this device, and severely limits its utility as a pulse delayer. If the expected diffusion constant governed the spreading, we could expect the width increase, under the same conditions of operation, to be

(23)

$$\Delta W_t = \frac{\sqrt{11.1 D_n t_o}}{v} \cong 19 \text{ nsec}$$

And under extremely ideal conditions $\mu = 1000$ cm^2/volt-sec, $v=10^6$ cm/sec, $t_D = 70$ nsec, we would expect:

$$\Delta W_t \cong 5 \text{ nsec}$$

which would allow the passage of very narrow pulses with minimum attenuation.

An estimate of the effective lifetime of electrons in the device can be obtained from Figure 13. This is a plot of peak current out, over peak current in, for E1, E2, E3, as a function of delay. A reasonably good fit is obtained if the theoretical curve (Figure 2-e) with 100 nsec assumed lifetime, is superimposed on the data. This reduction of lifetime to the order 100 nanoseconds is probably the re-

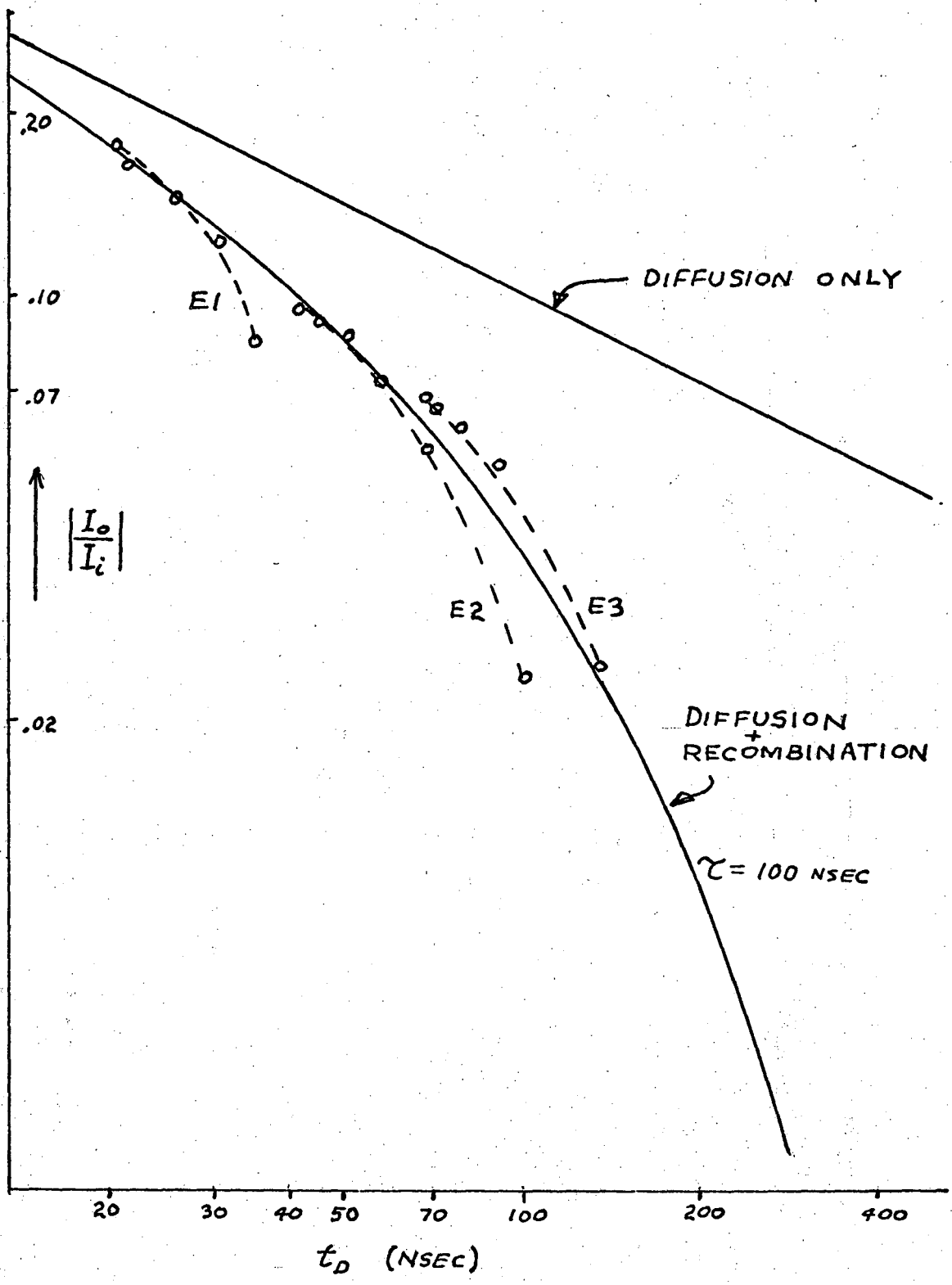

FIGURE 13: ATTENUATION - VS - DELAY

sult of a very high recombination rate at surface of the device. Better surface treatment would be necessary if one wished to build a device with delays approaching the microsecond range with reasonable attenuation. This shorter-than-expected lifetime limited the useful area of the device to the first three emitters since attenuation from the fourth and fifth emitters was too great for accurate measurements to be taken.

Interesting and useful properties are contained in the frequency response of the device. Figure 14 shows frequency response curves for E1, E2, and E3 at different drift field settings. Bandwidths vary from a minimum of about 3.5 MHz at E3 (V=8v) to about 8 MHz at E1 (V=17v). Roll-off slopes vary from about 6 db/octave to about 18 db/octave at the two extremes. Midband current gain varies from about 0.3 to 0.6. Phase shift measurements for E2 indicate that 180° phase shift occurs along a locus of points covering a ratio of 3 to 2 in frequency and 2 to 1 in amplitude. This property of providing 180° phase shift with current gains of about 0.1 to 0.2 indicates the possibility of using the device in a phase-shift oscillator.

It is interesting to compare the measured frequency response, both in amplitude and phase, with that predicted by the theory of an ideal device. If the values of t_D and W obtained from pulse measurements are inserted into the frequency function, very good agreement results. Figure 15 shows the theoretical and measured response for E2, V=10

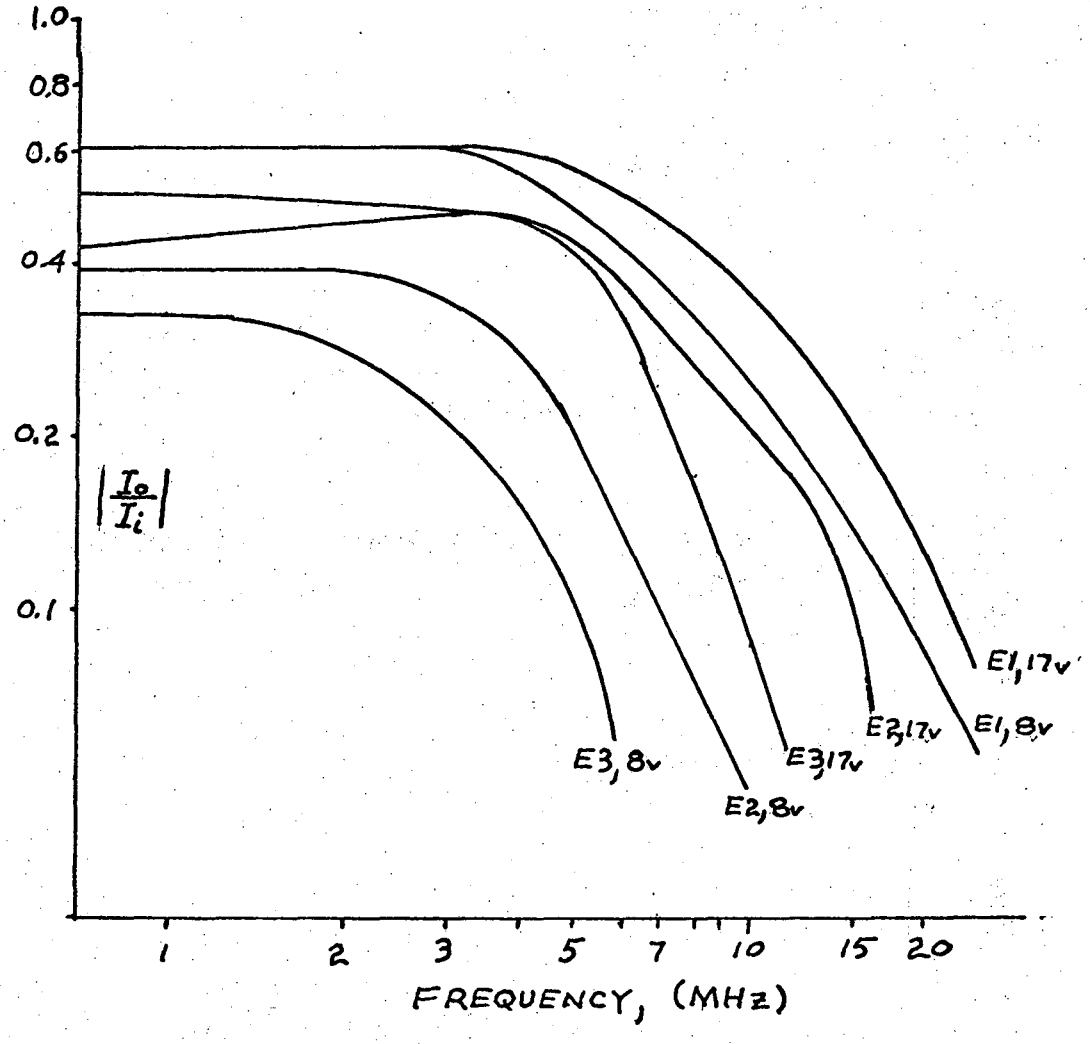

FIGURE 14: FREQUENCY RESPONSE, FOR INJECTION AT E1, E2, E3

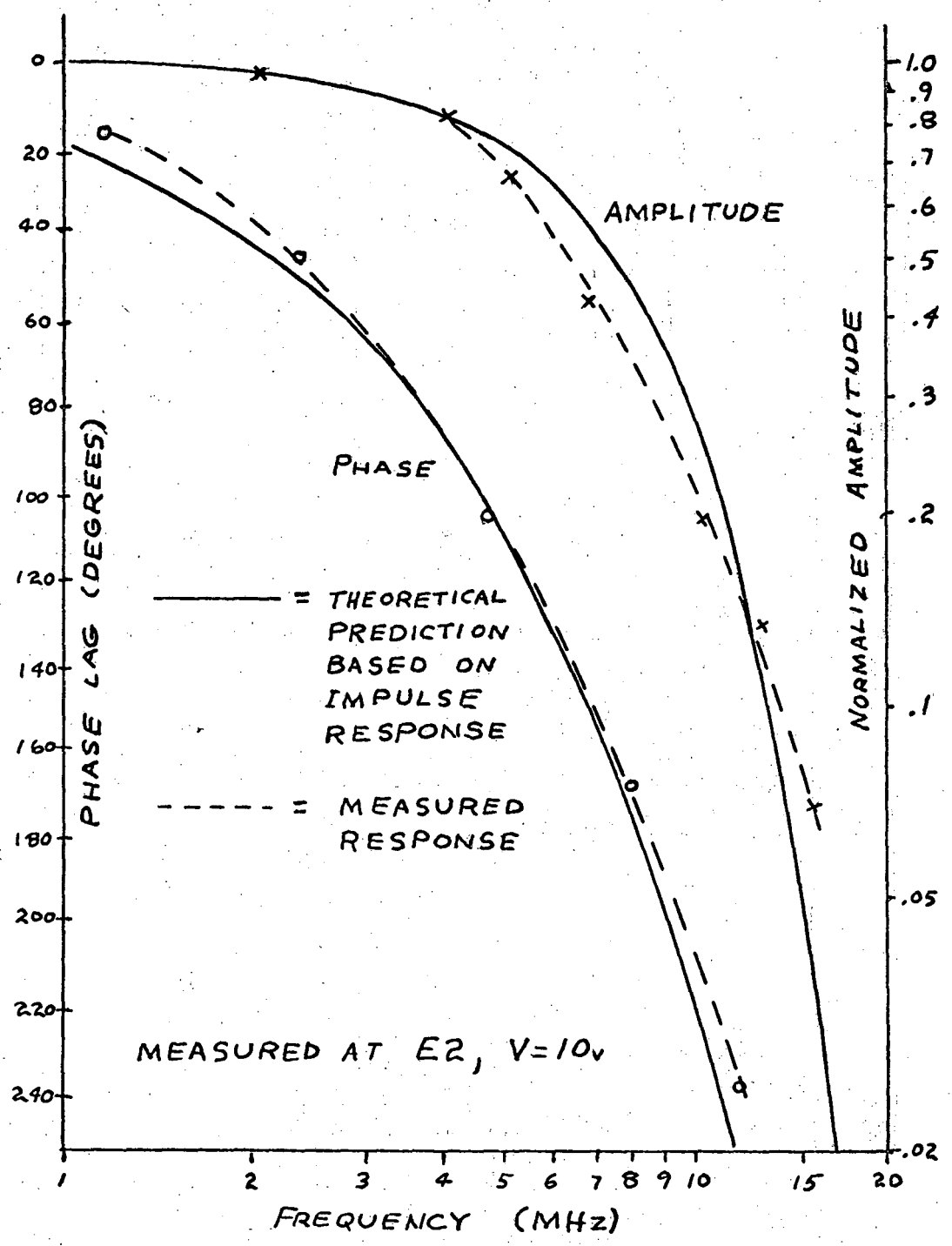

FIGURE 15: THEORETICAL AND MEASURED FREQUENCY RESPONSE

volts. The greatest disagreement comes in the amplitude characteristic, but this is to be expected, since the observed impulse response is obviously not a pure gaussian. It should be pointed out that the theoretical phase characteristic is exactly linear with frequency, and the measured characteristic agrees quite closely with this.

What would be the frequency performance to be expected from a device with the spreading reduced to 10 nanoseconds per 60 nanoseconds of delay by improving construction techniques and eliminating the anomalies present in the existing device? Calculations for this case, which represents the highest argument tabulated by Fried and Conte, indicates a bandwidth of the order of 200 MHz with extremely fast roll-off.

THERMAL CHARACTERISTICS

The temperature dependence of mobility represents one of the major problems confronting the application of minority carrier delay devices. The rapid decrease of mobility with increasing temperature causes delay to increase with ambient temperature, and also with self-heating.

A device was arranged as shown in Figure 16. The field was produced by injecting a known current into the ohmic contacts, instead of maintaining a constant voltage across the device. If delay is inversely proportional to electric field, and the temperature dependence of minority and majority mobilities is the same, then, as shown in (41), the delay should be constant with temperature. However, the delay was found to be proportional to $(V)^{-1/2}$ in the pulsed device where temperature was constant. Therefore, as should be expected, the current biasing did not provide enough compensation for temperature change.

Delay was measured by injecting a sinusoidal waveform, and measuring the frequency required to give 180° phase shift. All measurements were made at E2. Figure 17 shows how delay increases with temperature for several different bias currents. From this graph it appears that a constant delay (represented by a horizontal line) could be maintained by increasing the bias current as the temperature increased. Figure 18 is a graph showing the measured bias required to maintain a constant delay, as a function of temperature. If a linearly increasing bias current could be automatically

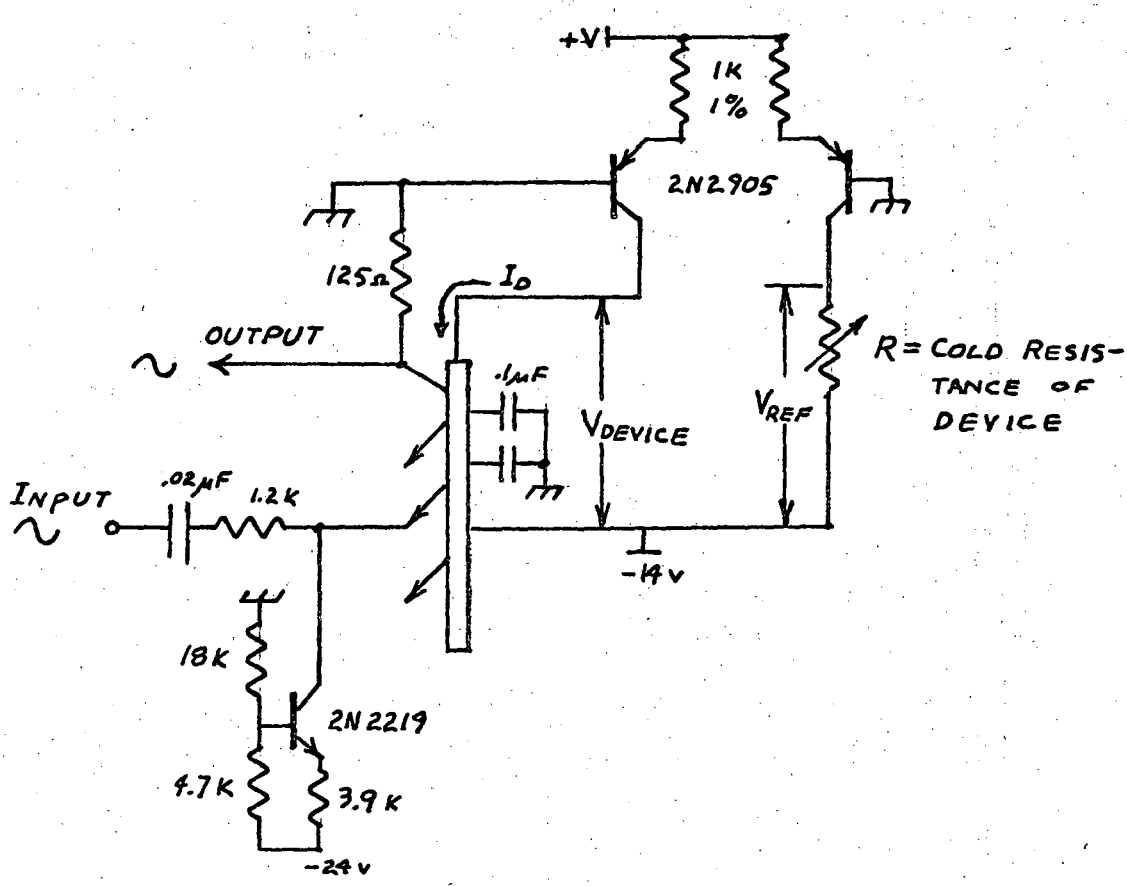

FIGURE 16: THERMAL TEST CIRCUIT

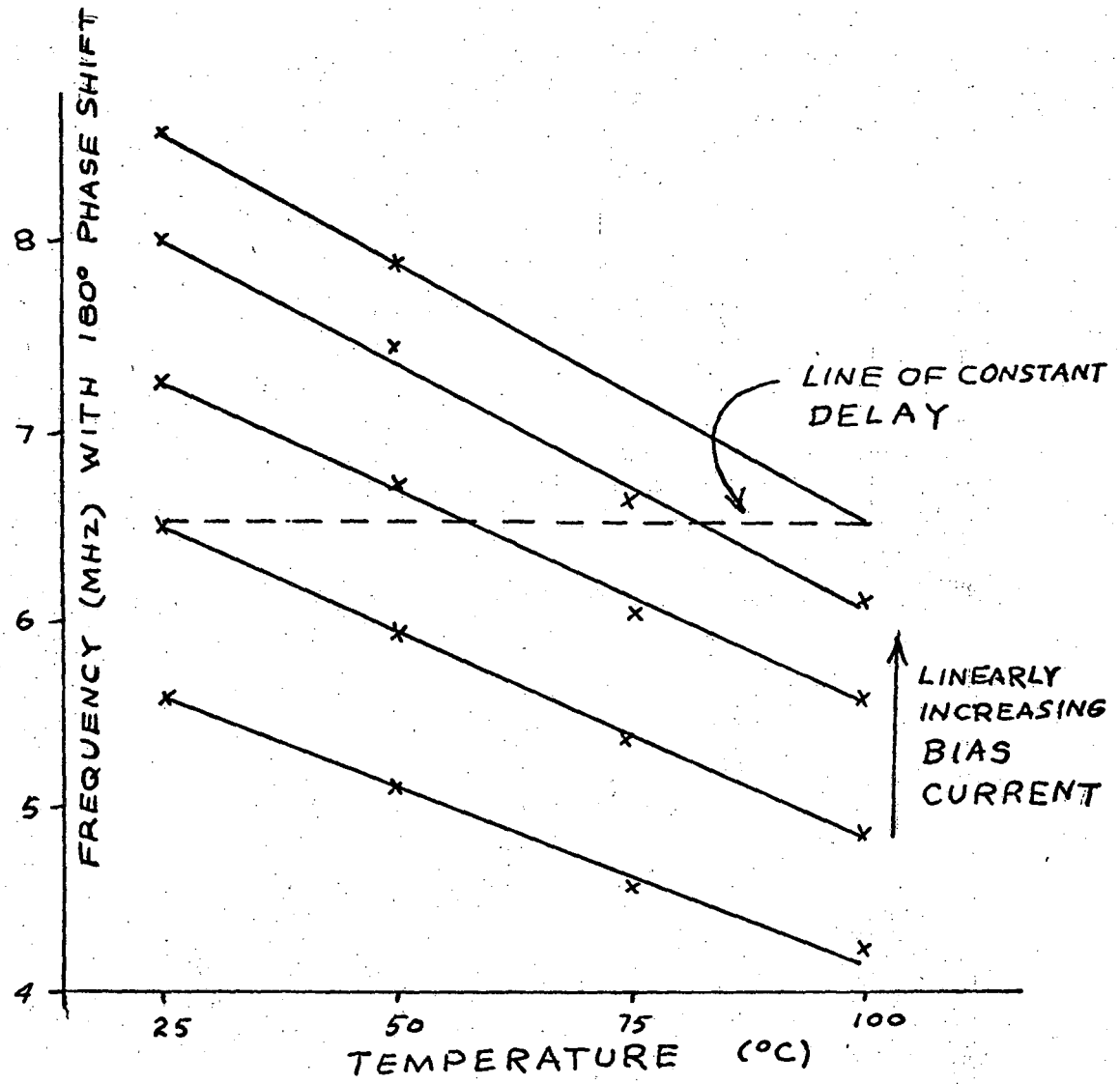

FIGURE 17: TEMPERATURE - DELAY CHARACTERISTIC

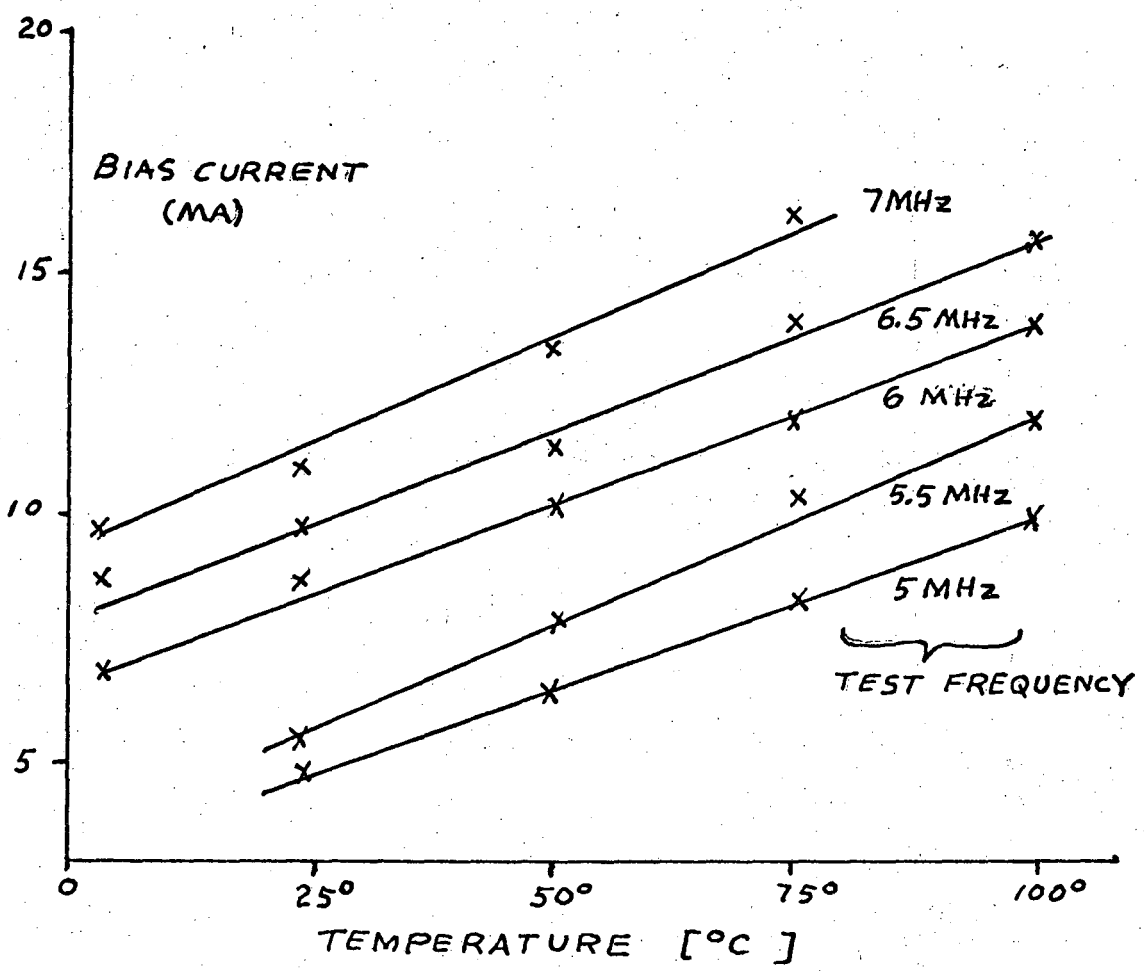

FIGURE 18: BIAS REQUIRED FOR CONSTANT DELAY - VS. - TEMPERATURE

produced, then the temperature dependence of delay could be compensated.

When the resistance between the ohmic contacts, R_d, was measured as a function of temperature, it was found to increase relatively linearly with both ambient temperature and bias current (Figure 19). This explains why the delay can be kept constant by a linearly increasing bias current. If $R_d \propto T$ and we must force $I \propto T$ to keep t_D constant, then

(43) $$V|_{t_D \text{ constant}} = I R_D \propto T^2.$$

This fact was also observed directly. Setting $t_D (V) \propto V^{1/2}$ equal to $-t_D (T) \propto T^{-1}$, as the condition for temperature compensation, and solving, we get $V \propto T^2$, which agrees with the experimental observation expressed in (43).

The amplitude, whose theoretical temperature dependence is very complicated, is found to be relatively insensitive to temperature. With constant current bias the amplitude of the output signal decreases about 10% as the temperature increases from 0°C to 100°C.

Automatic compensation for temperature variation was accomplished using the circuit of Figure 20. The ohmic portion of the device, between B3 and the negative ohmic contact, was used as a temperature sensing resistor. As the temperature rise caused R_s to increase, the voltage V_s increased accordingly, since R_s was fed by a constant-current source. An increase in V_s caused an increase in I_D, through the amplifiers Q3 and Q1. The gain of these amplifiers was trimmed

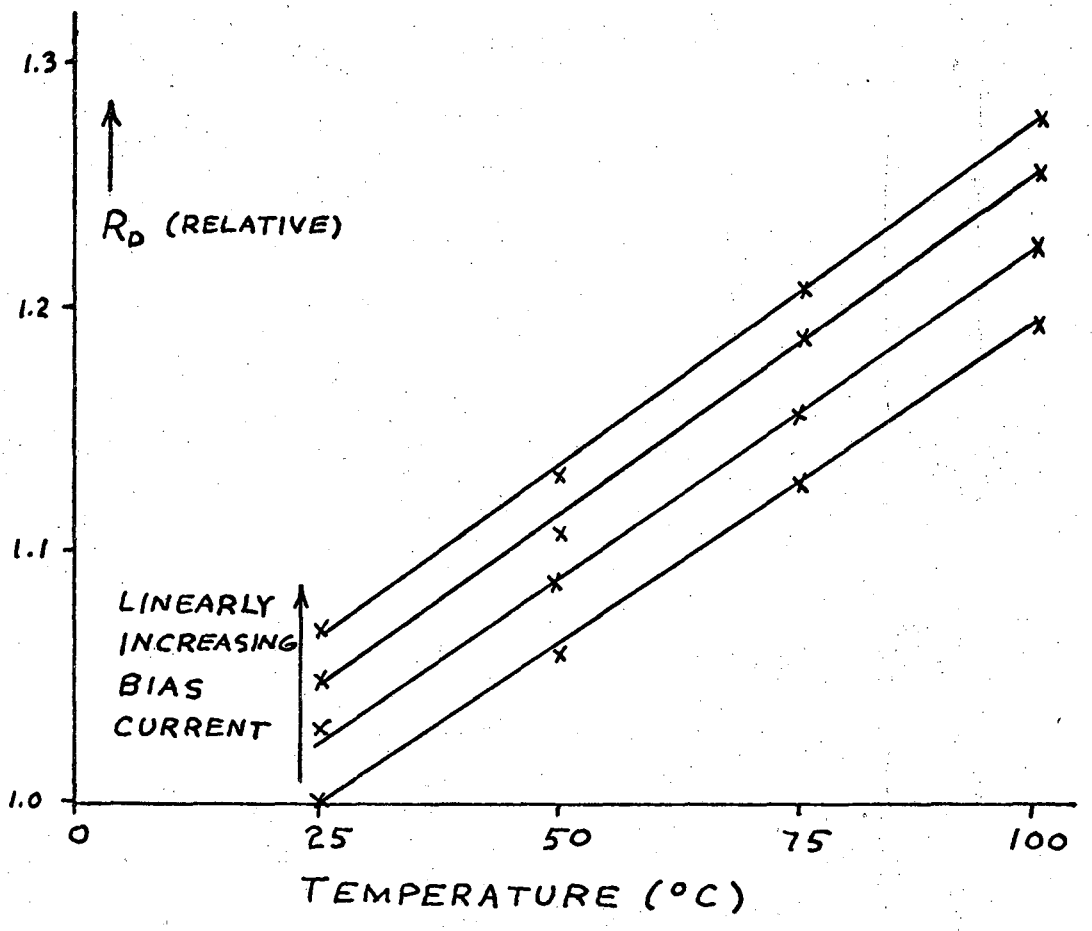

FIGURE 19: DEVICE RESISTANCE VS. TEMP.

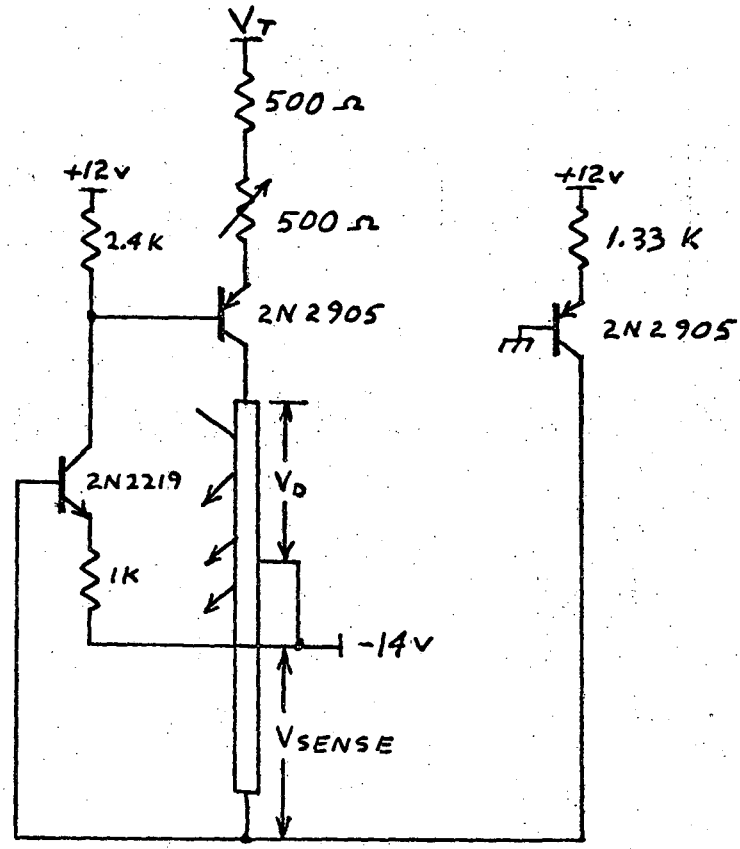

FIGURE 20 : TEMPERATURE COMPENSATION CIRCUIT

by R1 to compensate for the decreasing μ by increasing I_D appropriately. A variable control voltage, V_T, set the value of t_D. Thermal coupling between the active portion of the device and the sensing portion resulted in a positive feedback situation in the compensating loop, but the mechanism was perfectly stable over the range of 0°C to 100°C. The effectiveness of the temperature compensator was accurately measured by closing the signal loop between the collector and E2 with an inverting amplifier in signal path, thereby producing an oscillator whose frequency was proportional to $1/t_D$. The details of the oscillator are given later, but the temperature sensitivity of the oscillation frequency was $\pm$ 1% over the range 0°C to 100°C indicating very good compensation of the temperature dependent delay. Direct observations of pulse delay as a function of temperature were made which indicated the delay was, as expected, constant with temperature, although accurate measurements were not attempted.

APPLICATIONS

There are a number of possible applications for a device with controllable propagation delay. One such application is a variable nanosecond pulse delay element of the type used for fast coincidence systems in the study of particle physics. The quest for such a device served as the original impetus for this project, and although the device constructed falls far short of the bandwidth required for this application, future improvements could almost certainly achieve the required specifications. In principle, a nanosecond pulse delayer would work as shown in Figure 21. Coarse delay would be achieved by selection of one of the various inputs for injection of a standard pulse, and fine adjustment would be provided by variations of control voltage. The amplitude of current injected would be increased with distance, so that output amplitudes could be kept relatively constant. Differentiation of the input pulse results in a zero-crossing output signal suitable for amplitude-insensitive timing discrimination. This technique was actually tried on the experimental device with injection at E2 only. The delay was variable from 90 nsec to 120 nsec, with double-pulse resolution of about 125 nsec. Use as a practical nanosecond delay device would require resolution about an order of magnitude better than that achieved in this experimental device. Such an improvement is probably feasible with more sophisticated fabrication techniques than those used.

Two other time-delay applications with potential use-

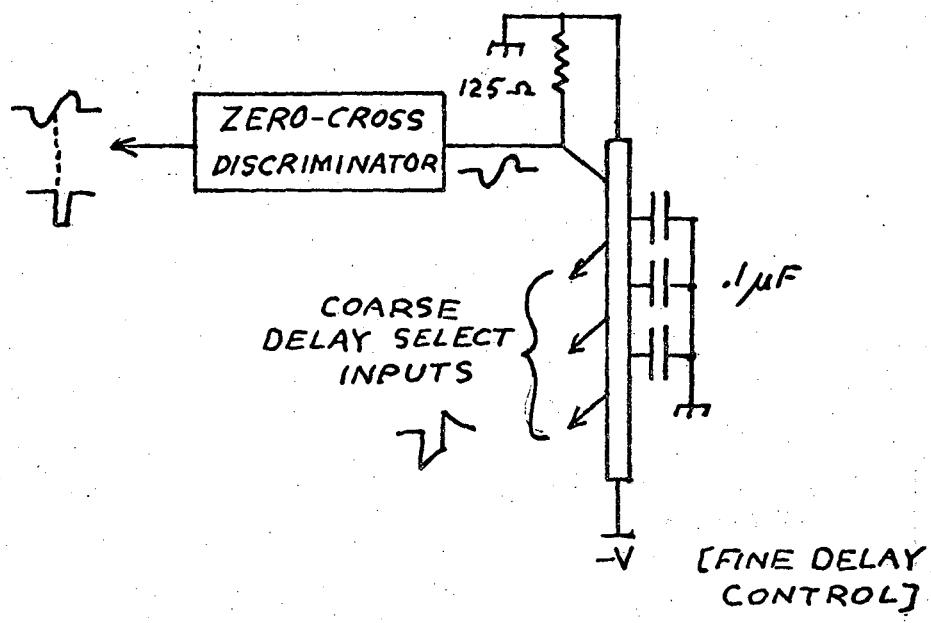

FIGURE 21: PULSE DELAYER

fulness would be: (1) Use of the variable risetime property to achieve controlled propagation delay in high-speed integrated circuit logic systems; and (2) Use of the energy-storage property to form a timing element in integrated monostable and astable multivibrators and dynamic shift registers.

Use of the phase shifting properties of this delay device led to the realization of several useful radio-frequency applications. Figure 22 shows a family of very nearly linear phase-shift versus frequency curves for several control voltages, measured at E2. Phase shifts as high as 360° were measured at E3. Application of a suitable signal to the control voltage input could produce a phase shift variation in excess of 45 degrees with this device.

Another obvious application for the phase-shift properties of this lateral transistor is for use in an oscillator. A single transistor feedback amplifier was used to form the oscillator circuit. The minimum gain required of such an amplifier is 5-10 in the range of interest, whereas a gain of about 30 is required for a conventional RC phase shift oscillator. Figure 23 shows the tuning characteristics of the oscillator, and Figure 24 shows the diagram of the oscillator used in this test and the temperature test reported in the previous section. As can be seen, the tuning characteristic is reasonably linear, and the temperature stability very good ($\pm$ 1% from 0°C to 100°C).

With the feedback amplifier adjusted to gain below

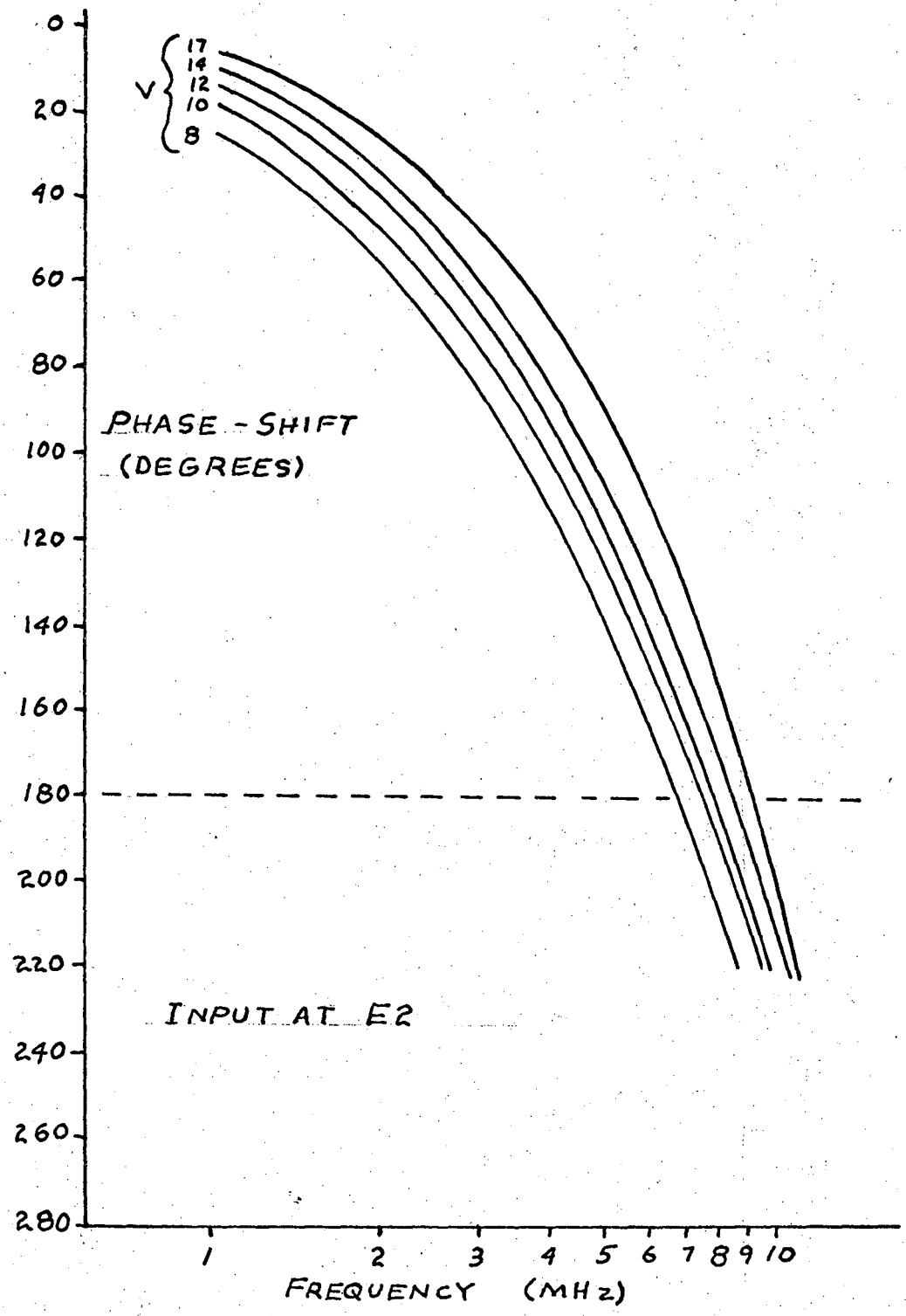

FIGURE 22 : PHASE - SHIFT CHARACTERISTIC

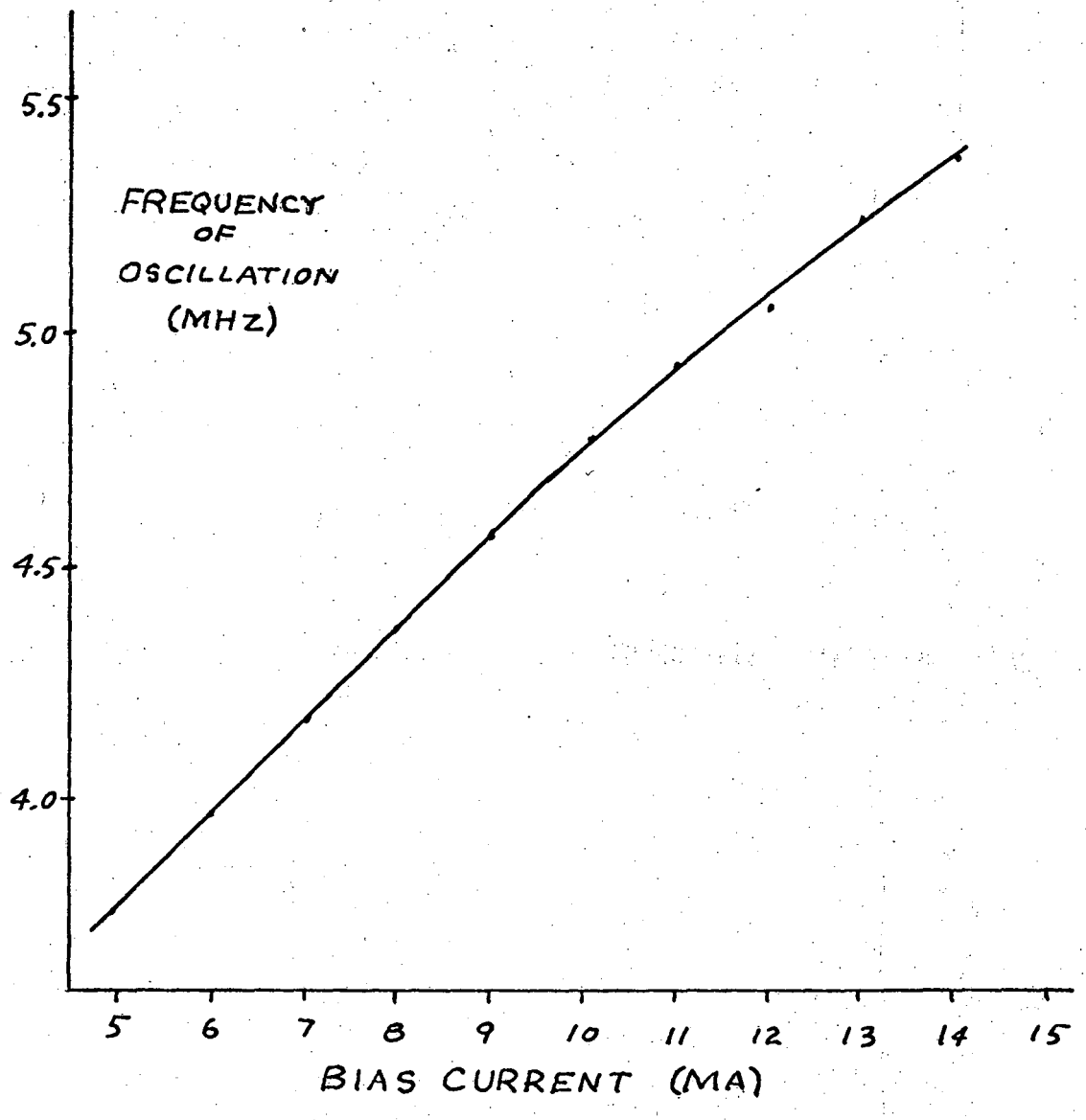

FIGURE 23: OSCILLATOR TUNING CHARACTERISTIC

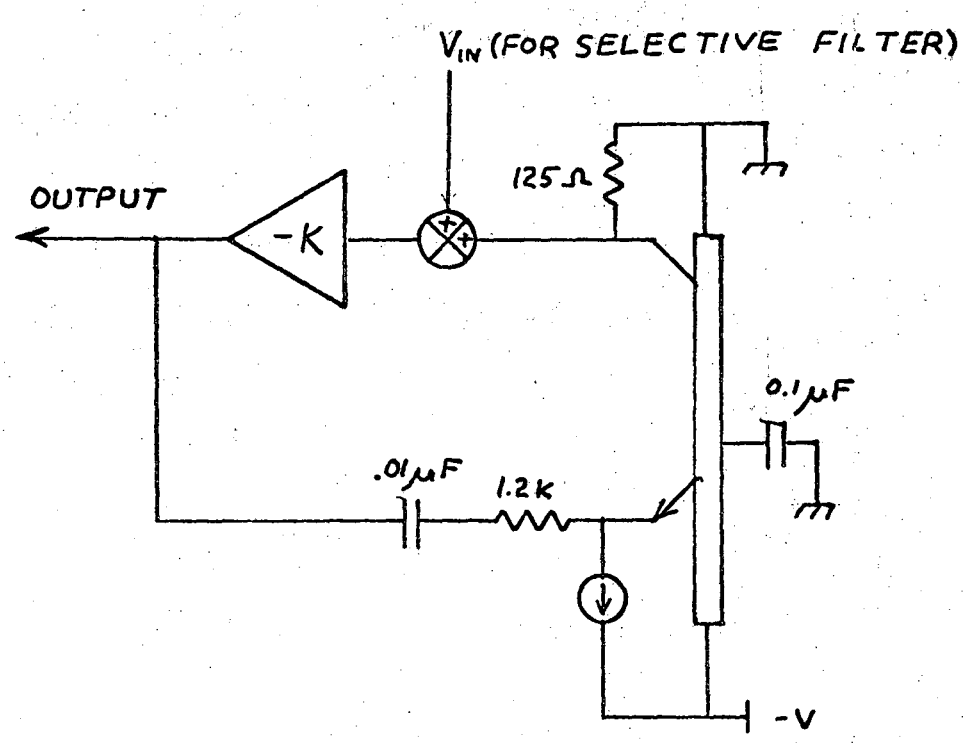

FIGURE 24: OSCILLATOR - SELECTIVE FILTER

CONCLUSION

The device described in this paper exhibited characteristics which conformed to theory quite well, except for two notable exceptions. The first anomaly was the fact that propagation velocity was proportional to the square root of applied voltage instead of being linearly related. The second anomaly was the larger-than-expected spreading of the pulse between input and output. There are possible explanations for these effects which are presented as hypothesis, since no experimental measurements were made which could prove or disprove their correctness.

The velocity anomaly could be explained if we assume that the mobility actually does change in the fashion indicated by the graph of "apparent mobility" in Figure 11. The apparent mobility changes from a maximum of about 900 at low field to 450 at high field. This might be explained if we assume that the majority current density gets high enough to cause conductivity modulation in the region where the minority carriers flow. A change in hole density from about 10^{16} to 10^{17} per cm^3 would account for the observed change in apparent mobility of electrons. The mobility of holes in this region would be decreased only about 20% as the majority concentration went from 10^{16} to 10^{17} atoms/cm^3. It is conceivable that such conductivity modulation could take place in the more lightly doped regions of the p-material and not show up very strongly in the V-I characteristic of the device because of the shunting effect of the heavily doped channel

region. This explanation would be consistent with the fact that minority carrier velocity is constant with distance for a given applied voltage, but falls below the expected increase with larger electric field. There is a square-root relationship between velocity and electric field predicted by Shockley[16], based on accoustical-mode phonon scattering. Some experimental tests of this effect using majority carriers show no appreciable non-linearity in silicon below 10^3 volts/cm.[17] More recent theoretical and experimental work shows the square-root relationship to be only approximate, and that a model including optical phonon scattering agrees more closely with experiment.[18]

The excess spreading of a pulse which gives an unexpectedly large value for the diffusion constant could actually be due to a collection time which is comparable to the pulse width. If minority carriers spread by diffusion to a depth below the n-type collector diffusion, they can still be collected by the force of the concentration gradient caused by the depletion of the electrons near the collector junction. Electrons would diffuse into the depletion region and be collected, but the result would be an artificial broadening of the received pulse.

The lateral transistor geometry used in this study was responsible for some of the limitations of the device. It can be stated, however, that the present device worked quite satisfactorily as phase-shifter. The main limitations affect the pulse delay capability, and perhaps some improve-

ment could be made in this regard within the limitations of the lateral geometry.

One possibility for realization of a better pulse delay device is in the geometry of Figure 26. This geometry, similar to that of a conventional transistor, but with an extremely wide base region, would feature an n-type collector and p-type ohmic contact on the bottom of the chip. Several advantages would be apparent. First, the electrons would travel in the bulk exclusively, thereby eliminating the problem of surface recombination. Second, the dimension of emitter and collector in the direction of electron travel would be extremely small, so that one and perhaps two sources of pulse spreading would be eliminated. Several fabrication problems exist, but the fabrication of such a device should certainly be possible, and would represent a logical extension of the work presented here.

The possibility of applying some of the results of this study to integrated circuit fabrication seems promising. Not only could the application of external drift field possibly aid the production of higher gain and frequency response lateral pnp transistors, but such possibilities as tunable phase-shift oscillators, phase modulators, phase detectors, and low-pass and band-pass filters are very interesting and merit further study.

Two avenues therefore appear open to future effort. One is the pulse delay device with conventional diffused transistor geometry, and the other is the assortment of linear applications in integrated circuits. Both areas

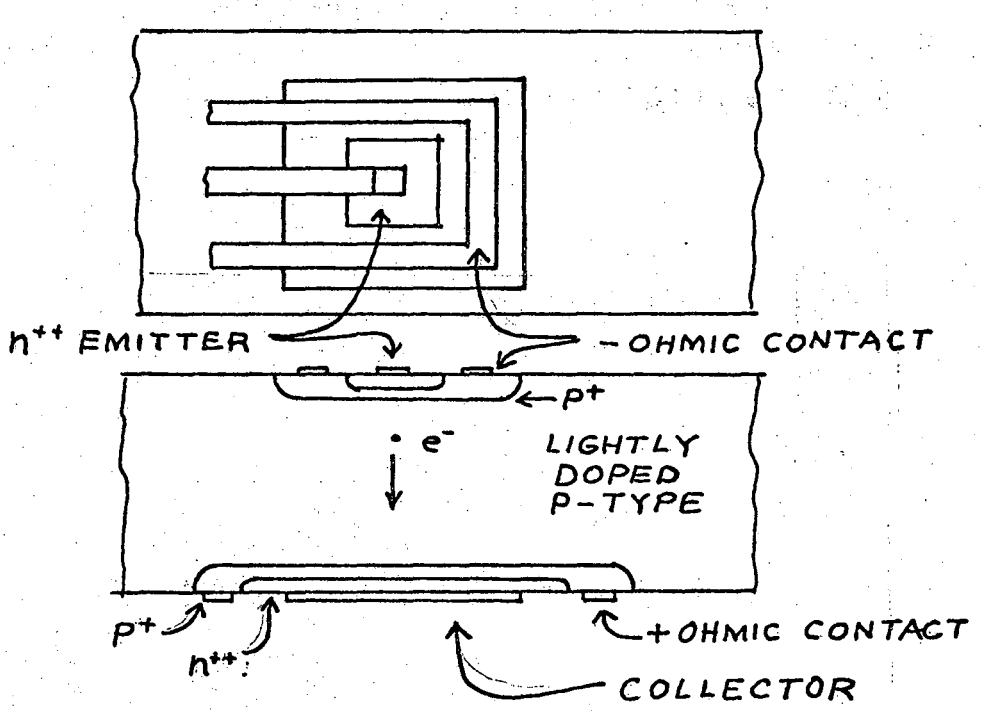

FIGURE 26: PROPOSED TRANSVERSE DEVICE GEOMETRY

offer promise of the eventual practical application of the phenomena first observed 20 years ago by Haynes and Shockley.

APPENDIX

Use of the Laplace-Transformed Gaussian in Frequency Response Calculations

Functions related to the Laplace-transformed Gaussian,

$$F(s-a) = e^{k^2(s-a)^2}\, erfc[k(s-a)]$$

are tabulated in Carslaw and Jaeger, Faddeyeva and Terent'ev, and Fried and Conte. The last reference is the most useful, since it tabulates the function for negative arguments, which is the range applicable to the problem at hand.

Fried and Conte define the function:[19]

$$F(z) = 2j\, e^{-z^2} \int_{-\infty}^{jz} e^{-t^2}\, dt$$

$$z = x + jy$$

Making use of the appropriate substitutions we can generate:

$$F(jz) = j\sqrt{\pi}\, e^{z^2}\, erfc\,(z)$$

The identification to the Laplace-transformed gaussian is simply:

$$F(jz) = j\sqrt{\pi}\, F(s-a)$$

Letting $s=j\omega$ for frequency response calculations,

$$z = -(ka) + j(k\omega)$$
$$jz = -(k\omega) - j(ka)$$

The following identities are given in the reference:

$$Re\ F[(-k\omega),(-ka)] = -Re\ F[(k\omega),(-ka)]$$

$$Im\ F[(-k\omega),(-ka)] = Im\ F[(k\omega),(-ka)]$$

which must be used because tables exist for

$x = k\omega$ positive only

$y = ka$ positive and negative (we use the negative portion)

So, when using the tables of F(z), the following rules apply:

1) $x = k\omega \qquad y = ka$

2) $Re\ F(s-a) = \sqrt{\pi}\ Im\ F(z)$

3) $Im\ F(s-a) = -\sqrt{\pi}\ Re\ F(z)$

4) For F(s-a), consult the table for $y \leq 0$ only.

As the authors point out, their table includes most reasonable values of the function for positive and negative arguments at intervals of 0.1 in x and y, which is sufficiently fine-grained for determining the function qualitatively by hand calculation.

It should be mentioned that F(s-a) represents the frequency domain solution to the base-transport problem in transistors, where an exponentially graded base doping profile is assumed. Use of this function could give a more accurate answer than the "Lumped Model" approach used in many texts.

FOOTNOTES

1. An exception to this is the negative resistance diode proposed by W. Shockley ("Negative Resistance Arising from Transit Time in Semiconductor Diodes", Bell System Tech. Jour., 33, 1954, pg. 799) and later, in the avalanche-drift form by W. T. Read ("A Proposed High-Frequency, Negative Resistance Diode" Bell System Tech. Jour., 37, 1958, pg. 401). This diode finds present-day practical application in microwave oscillators.
2. The basic theory in this section is derived from:
   R. B. Adler, et al., Introduction to Semiconductor Physics (Wiley, 1964) (Chapters 1, 3, and 4)
   S. Wang, Solid State Electronics (McGraw-Hill, 1966) (Chapters 3 and 5)
   A. S. Grove, Physics and Technology of Semiconductor Devices (Wiley, 1967) (Chapter 4)
3. R. M. Warner and J. N. Fordemwalt (Ed.) Integrated Circuits Design Principles and Fabrication (McGraw-Hill, 1965), pg. 35.
4. Grove, pg. 108
5. Adler, et al., Section 4.3
6. J. R. Haynes and W. Shockley "The Mobility and Life of Injected Holes and Electrons in Germanium", Physical Review, 81 - 5, 1951) pp. 835-843.
7. Adler, et al., pp. 174-175.
8. C. D. Hodgman (Ed.), C.R.C. Standard Mathematical Tables (1959), pg. 327.

9. Hodgman, pg. 334.

10. References to this function are:

H. S. Carslaw and J. C. Jaeger, Conduction of Heat in Solids (Clarendon Press, 1959), Appendix II.

V. N. Faddeyeva and N. M. Terent'ev, Tables of the Values of the Function

$$w(z) = e^{-z^2}\left(1 + \frac{2i}{\sqrt{\pi}}\int_0^z e^{t^2} dt\right.$$

(Pergamon Press, 1961)

B. D. Fried and S. D. Conte, The Plasma Dispersion Function, (Academic Press, 1961)

11. Plotted from data in Fried and Conte.

12. G. A. Rigby (Ed.), Integrated Circuits Laboratory Manual (unpublished).

13. Adler, et al., pg. 34.

14. Grove, Chapter 9.

15. Haynes and Shockley, pg. 836.

16. W. Shockley, "Hot Electrons in Germanium and Ohm's Law" Bell System Tech. Jour., 30, 1951, pg. 990.

17. E. J. Ryder,"Mobility of Holes and Electrons in High Electric Fields" Physical Review, 90, 1953, pg. 766.

and

E. C. Prior, "The Field-Dependence of Carrier Mobility in Silicon and Germanium" Journal Phys. Chem. Solids, 12. 1960, pg. 175.

18. E. M. Conwell, "Lattice Mobility of Hot Carriers" Journal Phys. Chem. Solids, 8, 1959, pg. 234.

19. The symbols used here are different than that used by Fried and Conte.

BIBLIOGRAPHY

Adler, R. B., Smith, A. C., Longini, R. L., Introduction to Semiconductor Physics (Wiley, 1964)

Carslaw, H. S., Jaeger, J. C., Conduction of Heat in Solids (Clarendon Press, 1959)

Conwell, E. M., "Lattice Mobility of Hot Carriers" Journal Phys. Chem. Solids, 8, 1959, pg. 234

Faddeyeva, V. N., Terent'ev, N. M., Tables of the Values of the Function $W(z) = e^{-z^2}\left(1 + \frac{2i}{\sqrt{\pi}}\int_0^z e^{t^2} dt\right)$ Fry, D. G. (translator) (Pergamon Press, 1961)

Fried, B. D., Conte, S. D., The Plasma Dispersion Function, (Academic Press, 1961)

Grove, A. S., Physics and Technology of Semiconductor Devices, (Wiley, 1967)

Haynes, J. R., Shockley, W. "The Mobility and Life of Injected Holes and Electrons in Germanium". Physical Review (Volume 81, No. 5, March 1, 1951) pp. 835-843.

Hodgman, C. D. (Editor) C. R. C. Standard Mathematical Tables, 12th Edition, (Chemical Rubber Publishing Co., 1959)

Prior, A. C., "The Field-Dependence of Carrier Mobility in Silicon and Germanium" Journal Phys. Chem. Solids, 12, 1960, pg. 175.

Read, W. T., "A Proposed High-Frequency, Negative-Resistance Diode" Bell System Technical Journal, 37, 1958, pg. 401.

Rigby, G. A. (Editor), Integrated Circuits Laboratory Manual (Electronics Research Laboratory, University of California, Berkeley, California, Unpublished, 1967)

Ryder, E. J., "Mobility of Holes and Electrons in High Electric Fields" Physical Review, 90, 1953, pg. 766.

Shockley, W., "Hot Electrons in Germanium and Ohm's Law" Bell System Technical Journal, 30, 1953, pg. 990.

Shockley, W., "Negative Resistance Arising from Transit Time in Semiconductor Diodes" Bell System Technical Journal, 33, 1954, pg. 799.

Wang, S., Solid-State Electronics (McGraw-Hill, 1966)

Warner, R. M., Fordemwalt, J. N., (Editors) Integrated Circuits Design Principles and Fabrication (McGraw-Hill, 1965)

ACKNOWLEDGEMENTS

I would like to thank Dr. Graham A. Rigby for suggesting this project, and for his guidance during the work.

Special thanks are due Mr. Fred Kirsten, of Lawrence Radiation Laboratory, Berkeley, for his cooperation and encouragement of this study.

Personal thanks to Mrs. Helen Poucher for help in preparation of this manuscript, and to Patricia Van Tuyl for her infinite patience and understanding throughout this year of effort.

TECHNICAL INFORMATION DIVISION
LAWRENCE RADIATION LABORATORY
UNIVERSITY OF CALIFORNIA
BERKELEY, CALIFORNIA 94720